National Aeronautics and Space Administration

ANALYTC

ROSAT

ANNUAL STATUS REPORT

FOR NASA GRANT NAG 5-1935

Submitted by: The Trustees of Columbia University
in the City of New York
Box 20, Low Memorial Library
New York, New York 10027

Prepared by: Columbia Astrophysics Laboratory
Departments of Astronomy and Physics
Columbia University
538 West 120th Street
New York, New York 10027

Title of Research: **"Diffuse Emission and Pathological Seyfert Spectra"**

Principal Investigator: Jules P. Halpern
Associate Professor of Astronomy

Period Covered by Report: 1 November 1994 - 31 October 1995

TABLE OF CONTENTS

NO X-RAY–LUMINOUS STARBURSTS IN THE *EINSTEIN* MEDIUM SENSITIVITY SURVEY, EITHER

JULES P. HALPERN[1], AND DAVID J. HELFAND
Columbia Astrophysics Laboratory, Columbia University,
538 West 120th Street, New York, NY 10027;
jules@carmen.phys.columbia.edu,
djh@carmen.phys.columbia.edu

AND

EDWARD C. MORAN
Institute of Geophysics and Planetary Physics,
Lawrence Livermore National Laboratory, L-413, Livermore, CA 94450;
edhed@igpp.llnl.gov

Submitted to *The Astrophysical Journal*

Received _____; *accepted* _____

[1] Visiting Astronomer, Kitt Peak National Observatory, National Optical Astronomy Observatories, which is operated by AURA, Inc., under a cooperative agreement with the National Science Foundation.

ABSTRACT

We continue to investigate recurrent claims that a substantial number of "normal" star-forming galaxies may have X-ray luminosities in the range 10^{42-44} ergs s^{-1}. In this installment, we present new spectra of four such emission-line galaxies that were ambiguously classified in the *Einstein* Extended Medium Sensitivity Survey (EMSS), and find that they all have intermediate-type Seyfert nuclei as evidenced by broad components of their Hα lines. We argue that any of the remaining emission-line galaxies in the EMSS with $10^{42} < L_X < 10^{44}$ ergs s^{-1} that were flagged as needing further spectroscopic work are almost certain to have active nuclei as well. We conclude that in these as well as other samples of X-ray-selected emission-line galaxies, X-ray luminosities in excess of 10^{42} ergs s^{-1} can and should be attributed to an active nucleus, even in the case that most of the infrared continuum or optical emission-line luminosity is caused by star formation. There is as yet no good evidence for X-ray-luminous starbursts.

Subject headings: galaxies:active – galaxies: Seyfert – galaxies: starburst – X-rays: galaxies

1. INTRODUCTION

Although the vast majority of emission-line galaxies with X-ray luminosities in excess of 10^{42} ergs s^{-1} are Seyferts, speculation recurs that some of these might be "normal" star-forming galaxies (Fruscione & Griffiths 1991; Boller et al. 1992; Boller, Fink, & Schaeidt 1994; Boyle et al. 1995; Griffiths et al. 1995). These proposals are motivated in part by the need to find a populous new class of X-ray emitters to constitute the X-ray background. Candidates for such X-ray luminous starbursts are usually drawn from large programs to identify X-ray sources, which rely upon optical spectra. Some of these spectra are inevitably of insufficient quality to demonstrate conclusively the presence or absence of a Seyfert nucleus, the signature of which can be quite subtle. And some are simply misidentifications of the X-ray source.

It is useful to examine candidate starbursts in a variety of X-ray-selected samples, because of the possibility that photoelectric absorption might greatly alter the number of such objects visible as a function of the X-ray energy bands covered by these surveys. We recently reobserved nearly all such candidates from the *ROSAT/IRAS* All-Sky Survey of Boller et al. (1992), and found, after rejecting several misidentifications, that the remaining "starburst" galaxies that have $L_X > 10^{42}$ ergs s^{-1} invariably harbor previously unrecognized Seyfert nuclei (Moran, Halpern, & Helfand 1994, 1995). A similar upper limit to the X-ray luminosity of starburst galaxies is apparent in the *Einstein/IRAS* survey of David, Jones, & Forman (1992). In this paper, we present new spectra of four selected emission-line galaxies with high X-ray luminosity that were ambiguously classified in another sample, the *Einstein* Extended Medium Sensitivity Survey (EMSS) of Stocke et al. (1991), and find that they all have Seyfert nuclei as revealed by broad bases on their Hα lines. We use these and previous results to formulate simple guidelines for interpreting the origin of the X-rays in galaxies which may show evidence for both a stellar and a non stellar origin of their optical emission lines. We restrict the discussion to star-formation and nuclear activity in spiral galaxies, thereby excluding the elliptical and S0 galaxies in which the emission lines are attributed to cooling flows.

2. SAMPLE SELECTION AND OBSERVATIONS

We drew our targets from among the 12 sources listed in the EMSS as having ambiguous classification as either normal spiral or AGN (Table 8 of Stocke et al. 1991). Two of these have X-ray luminosities less than 3×10^{41} ergs s^{-1}, and no sign of nuclear activity according to Stocke et al. (1991). We consider these to be plausible starburst X-ray sources and concentrate our attention instead on the remaining 10 objects with $L_X \gtrsim 10^{42}$ ergs s^{-1}. Of these, NGC 4156 and NGC 3884 were previously classified as low-ionization nuclear emission-line regions (LINERs) based on spectra in Elvis et al. (1981) and Reichert et al. (1982), respectively, and we consider them to be reliably documented active galactic nuclei (AGNs) based on information contained in those and subsequent studies (e.g., Filippenko & Sargent 1985; Huchra & Burg 1992). Two more objects from their Table 8 are almost certainly AGNs according to Stocke et al. (1991), and one is a secondary X-ray identification because of the presence of a cluster of galaxies in the field. Therefore, we judge that only five X-ray sources remain in this list as plausible candidates for X-ray luminous starbursts.

Four out of five of these candidates were available in the sky in 1995 January, and we observed them using the Goldcam CCD spectrometer on the KPNO 2.1 m telescope. The basic properties of the galaxies are listed in Table 1. Magnitudes and X-ray luminosities were taken from Stocke et al. (1991), while the redshifts and classifications are from our own spectra. Finding charts are available in Maccacaro et al. (1994). A resolution of 4.2 Å was achieved using a 600 lines mm^{-1} grating blazed at 6750 Å, and a slit width of 1″.8. The wavelength range covered was 5500–8500 Å. This setup was chosen to optimize the sensitivity to subtle features in the profile of the Hα line, which in X-ray-selected Seyferts is sometimes the only line in the visible spectrum to show evidence of nuclear activity. Absolute line fluxes are uncertain by at least 50% because a narrow slit was used, and because the sky was not photometric during most of the observing run.

3. SPECTROSCOPIC RESULTS

A summary of the spectroscopic results is given in Table 2, and the spectra around Hα are shown in Figure 1. All four targets show unambiguous evidence of Seyfert nuclei in their spectra. The most conclusive proof is the presence of a broad base on the Hα line in each case. Therefore, they must all be regarded as at least Seyfert 1.9 galaxies by the standard criteria, possibly becoming Seyfert 1.8 if their (unobserved) Hβ lines have broad components as well. Even the weakest broad component, in MS 1058.8+1003, is clearly evident; Gaussian components that fit the forbidden lines and narrow Hα leave a broad residual with FWHM $\sim$ 4600 km s^{-1} and flux that is $\sim$ 38% of the flux of narrow Hα.

Secondary indicators of Seyfert activity are emission-line widths in the narrow components that exceed 300 km s^{-1}, [N II]λ6583/Hα ratios greater than 0.5, and strong [O III], [O I] or [S II] lines (e.g., Veilleux & Osterbrock 1987), although no single one of these is either necessary or sufficient for such a classification. [O I]λ6300 is often non-Gaussian and broader than the other forbidden lines in Seyfert galaxies, presumably because of its higher critical density for de-excitation. Most of these additional characteristics are possessed by our spectra, but there is one interesting exception. The line widths in MS 1047.3+3518 are only 210 km s^{-1} after correcting for instrumental resolution, and its [O I] line is fairly weak. Therefore, if it were not for its broad Hα component, this spectrum might have been interpreted as a low-excitation H II region. Stocke et al. (1991) called both MS 1047.3+3518 and 1058.8+1003 probable Seyfert 2 galaxies because they did not detect the broad Balmer-line components. With our detections of broad Hα, however, the intermediate Seyfert classifications in Table 1 are preferred.

MS 1114.4+1801, the faintest and most distant of our objects, is distinguished by the relatively small equivalent widths of its lines, which are superposed on a continuum consisting partially of starlight from an early stellar population. Na I λ5892 absorption and TiO bands near 6250 Å and 7050 Å are apparent (as they are in our other objects as well). Since the broad Hα flux dominates over narrow Hα in this case, we tentatively give MS 1114.4+1801 a Seyfert 1.5 classification. Further information from the Hβ line is not likely to be forthcoming because Stocke et al. (1991) noted that it was undetected in their spectrum. It is fairly common for X-ray selection to call attention to weak Seyfert nuclei such as this one, even in relatively nearby galaxies such as NGC 4156 and NGC 3884 mentioned above, and NGC 3147 and NGC 4619 from the *ROSAT* All-Sky Survey, the latter two shown by Moran et al. (1994, 1995) to be a Seyfert 2 and a Seyfert 1, respectively. These may all be cases in which the nucleus is significantly reddened, as we have discussed elsewhere (Moran et al. 1995).

4. DISCUSSION

In fairness to Stocke et al. (1991), we should emphasize that those authors fully expected that their ambiguous objects would turn out to be Seyferts if and when better spectra were taken. Suggestions that they might instead be starbursts have been promulgated by others, in our opinion, without adequate justification. For example, a search for starburst X-ray sources among the EMSS and other *Einstein* sources was carried out by Fruscione & Griffiths (1991). They observed the one object from Table 8 of Stocke et al. (1991) that was not available during our run, MS 2348.6+1956, and these papers disagree about the classification, with Stocke et al. favoring a Seyfert 2, and Fruscione & Griffiths a starburst. Unfortunately, neither paper displays the actual spectrum. Of the remaining four starburst X-ray sources claimed by Fruscione & Griffiths, none exceed 10^{42} ergs s^{-1} in X-ray luminosity. And suspiciously, one of the "starburst" spectra they did display, of the source IPC 0400.1–1811, shows an obvious broad Hα component that was not remarked upon by them. It clearly has a Seyfert 1.9 nucleus. Similarly, a *ROSAT/IRAS* source (1556.4+6359) classified by Boller et al. (1994) as an H II galaxy based on a low-resolution spectrum, is actually a Seyfert 1.8 (Moran et al. 1995). We conclude that these investigations, like ours, demonstrate an absence of evidence for X-ray luminous starbursts.

Perhaps a more interesting result is that not only are these objects Seyfert galaxies, they are all *broad-line* Seyferts. The paucity of Seyfert 2 galaxies with soft X-ray luminosities greater than 10^{42} ergs s^{-1} was noted by Halpern & Oke (1987) for optically selected samples, and by Stephens (1989) for X-ray-selected samples. Apparently, this conclusion continues to hold. In addition to

the results here, Moran et al. (1995) found that of the 209 objects that they classified from the *ROSAT/IRAS* All-Sky Survey, 15 are Seyfert 2 galaxies, and only six of these have $L_X > 3 \times 10^{42}$ ergs s^{-1}. From our experience, it is likely that some of these more luminous Seyfert 2 galaxies would reveal broad-line components as well if their starlight-dominated continuua are carefully subtracted.

In the context of Seyfert unification models based on obscuration and scattering, it is natural that detection of Seyfert 2 galaxies is disfavored by soft X-ray selection, as the direct flux is completely absorbed, while the scattered luminosity is roughly two orders of magnitude fainter than the intrinsic value. Of course, this deficit is also consistent with a model in which Seyfert 2s are intrinsically weaker X-ray sources than Seyfert 1s. X-ray spectra at higher energies can discriminate between these alternatives. The broad Hα components themselves could reveal which model best applies, through spectropolarimetry and variability studies. It is known that the broad-line components in most Seyfert 1.8 and 1.9 galaxies are reddened, and often highly variable on timescales of years, which can be attributed to partial and variable obscuration in and around the broad-line region (Goodrich 1989; 1995). In contrast, the broad lines in hidden Seyfert 1 nuclei that are detected only with spectropolarimetry are constant, and not particularly reddened, presumably because they are viewed indirectly via a large, warm electron-scattering region. We expect that the spectra presented here are probably of the former, directly viewed variety, precisely because we can detect them without using spectropolarimetry. Of the 10 Seyfert 2 nuclei with polarized broad lines studied by Tran (1995), only one, Was 49b, also shows the broad components in its direct spectrum (Moran et al. 1992). Furthermore, it is possible that long-term variability can contribute to the failure of previous spectroscopy to detect the broad-line components which we have found.

In order to compare the properties of these objects with those of "normal" Seyfert galaxies, one would first like to know how their broad Hα line luminosities compare with those of Seyfert 1 galaxies of the same X-ray luminosity. Using the data in Tables 1 and 2, we find that the ratio of L_X to broad Hα ranges from 10 to 130, with an arithmetic mean of 48. Surprisingly, this is very close to the mean ratio of 40 determined by Elvis, Soltan, & Keel (1984) using 2–10 keV luminosities of a hard X-ray-selected sample of Seyfert 1 galaxies. The closeness of these two mean values is surely fortuitous, as our emission-line luminosities are uncertain by at least 50% and the X-ray sources probably vary by at least this factor as well. Despite the softer X-ray energies, and the likely partial obscuration that may affect the broad-line region differently from the X-ray continuum source, it nevertheless appears that the principal manifestations of Seyfert activity emerge in basically their normal proportions.

Given the ubiquity of Seyfert nuclei in galaxies with X-ray luminosities in the range $10^{42} - 10^{43}$ ergs s^{-1}, it seems unlikely that X-ray sources even more luminous than these are starbursts. Nevertheless, Boyle et al. (1995) suggest that up to 24 additional objects with $L_X > 10^{43}$ ergs s^{-1}, from Table 10 of Stocke et al. (1991), are plausible candidates for starbursts. In fact, Boyle et al. claim that two of these actually *are* H II region galaxies with X-ray luminosities of 2.2×10^{43} and 1.3×10^{44} ergs s^{-1}, although the new spectra on which they base this conclusion are not shown. Since these galaxies are considerably fainter ($V = 18.7, 19.3$) than the ones we have studied, and are at higher redshift ($z = 0.139, 0.198$), we remain skeptical that they lack AGNs until we can evaluate high-quality spectra of their Hα regions. Similarly, Griffiths et al. (1995) speculate that two faint *ROSAT* sources at even higher redshift ($z = 0.312, 0.253$) could be starbursts with $L_X \sim 10^{43}$ ergs s^{-1}. However, they do acknowledge that the as yet unobserved Hα lines in their objects might reveal weak broad components indicative of obscured Seyfert activity, a prediction which we heartily second.

One sure path to premature speculation about X-ray luminous starbursts is the reliance upon a single "global" classification of an emission-line galaxy using, for example, the line-ratio diagnostics of Veilleux & Osterbrock (1987), or a single measurement of FWHM. That these simple prescriptions are sometimes inadequate for determining the source of the X-ray emission should be apparent from the fact that many well-known active galaxies are composites, containing both Seyfert nuclei and star-forming regions. In cases where both phenomena are present in the spectrum in roughly equal amounts, standard line-ratio diagnostics are invalid, and often fail to recognize the Seyfert component. A composite emission-line spectrum also constitutes a warning that the *continuum*

emission in different wavelength bands may have different origins. For example, the far-infrared may be dominated by star formation, while the AGN may be responsible for the bulk of the X-ray emission. For the purpose of determining the sources of the various continuum components, then, it is obviously insufficient to classify an object merely as "a starburst galaxy," or "a Seyfert galaxy."

Examples of X-ray-emitting galaxies with nuclear spectra containing unresolved contributions from both emission-line mechanisms were explicitly demonstrated by Véron et al. (1981a), and Véron, Véron, & Zuidervijk (1981b). Their principal indicator that a Seyfert nucleus was hidden among normal H II regions was the presence of [O III]λ5007 *broader* than Hβ. The explanation of this phenomenon is obvious upon consideration of the relative velocity widths and [O III]/Hβ ratios in Seyfert nuclei versus H II regions. To this interesting clue, we add a reminder of the more common signature, namely, the broad base on Hα, and consider either of these indicators to be sufficient, as did Véron et al., to attribute the X-ray source to an active nucleus. Seven of these composite Seyfert/H II galaxies with high X-ray luminosities and [O III] broader than Hβ were discovered by Moran et al. (1995), probably because the addition of the infrared selection criterion in their sample favors those galaxies which also have substantial star formation. We refer the reader to that paper for detailed discussions of their properties and possible implications for the origin of the X-ray background.

5. CONCLUSIONS

The results of all these investigations can be summarized as follows: Among the 835 EMSS sources, and 241 sources in the *ROSAT/IRAS* All-Sky Survey, there is not yet a single well-certified example of a starburst whose X-ray luminosity is substantially in excess of 10^{42} ergs s^{-1}. All such candidates are found to have broad bases on Hα, and/or [O III] lines broader than Hβ, either of which can be attributed to the presence of an active nucleus. High-quality spectra of higher redshift candidates from *ROSAT* deep surveys are not yet available to make these same tests. Until they are, we favor the hypothesis that the X-ray emission in these cases originates in an AGN, possibly obscured, or possibly not. Future investigations of luminous X-ray emission-line galaxies should employ the two particular emission-line tests which we have discussed as the most sensitive indicators of an active nucleus. Both broad Hα and broad [O III] should be ruled out before attributing the X-rays to a non-AGN source. Whereas galaxies are usually presumed innocent of Seyfert activity until proven guilty, in cases where they have X-ray luminosities of 10^{42} ergs s^{-1} or more, the reverse is arguably the more judicious assumption.

This work was supported in part by NASA grant NAG 5-1935. This is Columbia Astrophysics Laboratory contribution 567.

TABLE 1
SUMMARY OF OBSERVATIONS

Name	V	z	log L_X (ergs s^{-1})	Date (1995 UT)	Time (s)	Class
MS 0942.8+0950	15.6	0.01337	42.49	Jan. 23	1800	Sy 1.9
MS 1047.3+3518	15.6	0.04125	42.82	Jan. 22	1800	Sy 1.9
MS 1058.8+1003	15.5	0.02717	42.20	Jan. 22	1800	Sy 1.9
MS 1114.4+1801	16.5	0.09205	42.61	Jan. 22	4200	Sy 1.5

TABLE 2
EMISSION-LINE FLUXES AND WIDTHS

Property	0942.8+0950	1047.3+3518	1058.8+1003	1114.4+1801
[O I]λ6300	0.10	0.06	0.10	0.47
[N II]λ6548	0.26	0.22	0.18	0.60
H$\alpha(n)$	1.00	1.00	1.00	1.00
H$\alpha(b)$	2.75	1.25	0.38	9.45
[N II]λ6583	0.77	0.67	0.54	1.66
[S II]λ6716	0.23	0.18	0.23	1.15
[S II]λ6731	0.25	0.16	0.21	0.86
H$\alpha(n)$ FWHM (km s^{-1})	300	210	310	380
H$\alpha(b)$ FWHM (km s^{-1})	2200	4800	4600	7700
H$\alpha(n)$ EW (Å)	18.	30.	33.	4.
H$\alpha(n)$ Flux (ergs cm^{-2} s^{-1})	1.1×10^{-14}	2.7×10^{-14}	5.9×10^{-14}	1.2×10^{-15}

REFERENCES

Boller, T., Fink, H., & Schaeidt, S. 1994, A&A, 291, 403

Boller, T., Meurs, E. J. A., Brinkmann, W., Fink, H., Zimmermann, U., & Adorf, H.-M. 1992, A&A, 261, 57

Boyle, B. J., McMahon, R. G., Wilkes, B. J., & Elvis, M. 1995, MNRAS, 272, 462

David, L. P., Jones, C., & Forman, W. 1992, ApJ, 388, 82

Elvis, M., Schreier, E. J., Tonry, J., Davis, M., & Huchra, J. P. 1981, ApJ, 246, 20

Elvis, M., Soltan, A., & Keel, W. C. 1984, ApJ, 283, 479

Filippenko, A. V., & Sargent, W. L. W. 1985, ApJS, 57, 503

Fruscione, A., & Griffiths, R. E. 1991, ApJ, 380, L13

Goodrich, R. W. 1989, ApJ, 340, 190

———. 1995, ApJ, 440, 141

Griffiths, R. E., Georgantopoulos, I., Boyle, B. J., Stewart, G. C., Shanks, T., & Della Ceca, R. 1995, MNRAS, in press

Halpern, J. P., & Oke, J. B. 1987, ApJ, 312, 91

Huchra, J., & Burg, R. 1992, ApJ, 393, 90

Maccacaro, T., Wolter, A., McLean, B., Gioia, I. M., Stocke, J. T., Della Ceca, R., Burg, R., & Faccini, R. 1994, Astrophys. Lett. Comm., 29, 267

Moran, E. C., Halpern, J. P., Bothun, G. D., & Becker, R. 1992, AJ, 104, 990

Moran, E. C., Halpern, J. P., & Helfand, D. J. 1994, ApJ, 433, L65

———. 1995, ApJS, submitted

Reichert, G., Mason, K., Thorstensen, J., & Bowyer, S. 1982, ApJ, 260, 437

Stephens, S. A. 1989, AJ, 97, 10

Stocke, J. T., Morris, S. L., Gioia, I. M., Maccacaro, T., Schild, R., Wolter, A., Fleming, T. A., & Henry, J. P. 1991, ApJS, 76, 813

Tran, H. D. 1995, ApJ, 440, 565

Veilleux, S., & Osterbrock, D. E. 1987, ApJS, 63, 295

Véron, P., Véron, M. P., Bergeron, J., & Zuidervijk, E. J. 1981a, A&A, 97, 71

Véron, P., Véron, M. P., & Zuidervijk, E. J. 1981b, A&A, 98, 34

FIGURE CAPTIONS

FIG. 1.– New spectra of EMSS sources, transformed to rest wavelength. The units of flux are 10^{-27} ergs cm^{-2} s^{-1} Hz^{-1}.

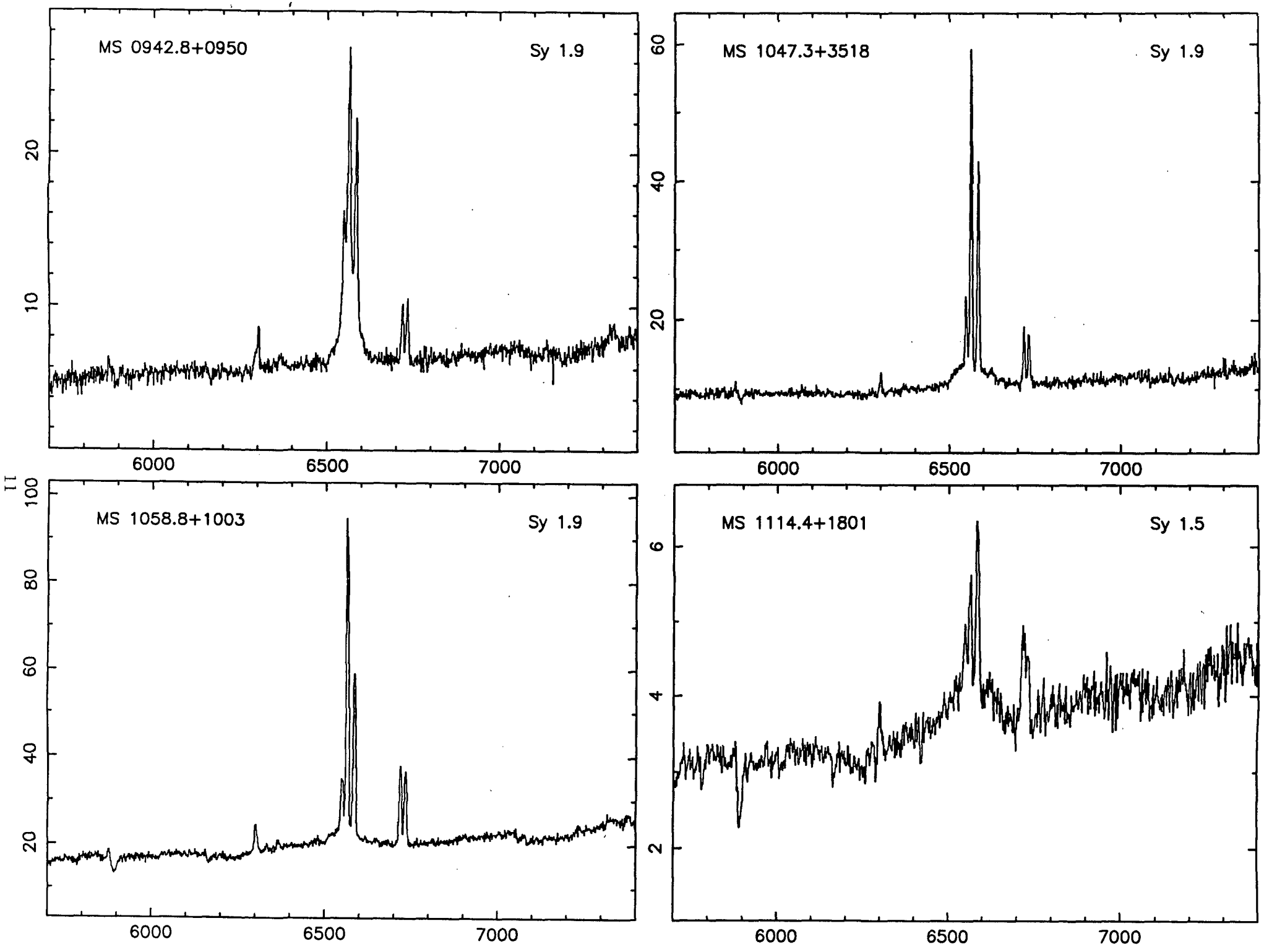
MS 0942.8+0950
Sy 1.9
MS 1047.3+3518
Sy 1.9
MS 1058.8+1003
Sy 1.9
MS 1114.4+1801
Sy 1.5
6000
6500
7000

N15

ROSAT PSPC and HRI observations of the composite starburst/Seyfert 2 galaxy NGC 1672

N96-13428

W.N. Brandt,[1] J.P. Halpern[2] and K. Iwasawa[1]

[1] *Institute of Astronomy, Madingley Road, Cambridge CB3 0HA (Internet: wnb@ast.cam.ac.uk, ki@ast.cam.ac.uk)*
[2] *Columbia Astrophysics Laboratory, Columbia University, 538 West 120th Street, New York, NY 10027 USA (Internet: jules@carmen.phys.columbia.edu)*

52-89
5565
p. 17

ABSTRACT

The nearby barred spiral galaxy NGC 1672 has been observed with the Position Sensitive Proportional Counter (PSPC) and High Resolution Imager (HRI) instruments on board the *ROSAT* X-ray satellite. NGC 1672 is thought to have an obscured Seyfert nucleus, and it has strong starburst activity as well. Three bright X-ray sources with luminosities $1\text{–}2\times10^{40}$ erg s^{-1} are clearly identified with NGC 1672. The strongest lies at the nucleus, and the other two lie at the ends of NGC 1672's prominent bar, locations that are also bright in Hα and near-infrared images. The nuclear source is resolved by the HRI on about the scale of the recently identified nuclear ring, and one of the sources at the ends of the bar is also probably resolved. The X-ray spectrum of the nuclear source is quite soft, having a Raymond-Smith plasma temperature of ≈ 0.7 keV and little evidence for intrinsic absorption. The *ROSAT* band X-ray flux of the nuclear source appears to be dominated not by X-ray binary emission but rather by diffuse gas emission. The absorption and emission properties of the sources, as well as their spatial extents, lead us to models of superbubbles driven by supernovae. However, the large density and emission measure of the nuclear X-ray source stretch the limits that can be comfortably accommodated by these models. We do not detect direct emission from the putative Seyfert nucleus, although an alternative model for the nuclear source is thermal emission from gas that is photoionized by a hidden Seyfert nucleus. The spectra of the other two X-ray sources are harder than that of the nuclear source, and have similar difficulties with regard to superbubble models.

Key words: galaxies: individual: NGC 1672 – galaxies: individual: NGC 1688 – galaxies: Seyfert – X-rays: galaxies.

1 INTRODUCTION

1.1 Basic facts

NGC 1672 (PKS 0444 − 593) is a $V = 10.1$ barred spiral galaxy of type SB(s)b. It is the principal galaxy in a group that is partially covered by the Large Magellanic Cloud, and a member of the Dorado cloud complex (see fig. 4 of de Vaucouleurs 1975). The radial velocity of NGC 1672 relative to the centroid of the Local Group is 1 140 km s^{-1} (Osmer, Smith & Weedman 1974; hereafter OSW74). It has *four* principal outer arms and these contain many H II regions 2–4 arcsec in size (Sandage & Bedke 1994). On deep optical photographs the arms can be seen to extend out to about 6 arcmin from NGC 1672's centre, although they become quite faint outside about 3 arcmin from the centre (cf. Sandage & Bedke 1994). Its bar has a length of 2.4 arcmin and vigorous star formation is seen at its ends (Baumgart & Peterson 1986), as is consistent with theoretical calculations of density enhancements associated with bars (see sect. 9 of Athanassoula 1992 and references therein). Conspicuous dust lanes are present along the leading edges of the bar (Baumgart & Peterson 1986). Elmegreen et al. (1991) suggested that NGC 1672 may have interacted with NGC 1688 and that this interaction may have led to NGC 1672's 'ocular' central shape. The centres of NGC 1672 and NGC 1688 are separated by 39 arcmin, and NGC 1688 is roughly one third as massive as NGC 1672. We shall adopt a Hubble constant of $H_0 = 50$ km s^{-1} Mpc^{-1} and a cosmological deceleration parameter of $q_0 = \frac{1}{2}$ throughout. This gives a distance to NGC 1672 of 22.8 Mpc (assuming the proper motion of NGC 1672 is small relative to its Hubble flow velocity). At this distance NGC 1672's bar is 16 kpc long and the HRI's spatial resolution (≈ 5 arcsec) corresponds to about 550 pc.

1.2 The nuclear region

The nucleus of NGC 1672 was noted to be peculiar by Sérsic & Pastoriza (1965). Pastoriza (1973) stated that it has dimensions of $\approx 22 \times 14$ arcsec with its longest axis lying in the Northeast direction. An isophotal map of the nuclear region can be found in Sérsic (1968). The nuclear spectrum has a polarization of ≤ 1.2 per cent in the B, R and H bands (Brindle et al. 1990). The relative strengths of the optical

emission lines in the spectrum taken through a 20 arcsec aperture are similar to those found in ordinary H II regions (OSW74), although sources of gas ionization in addition to normal OB stars cannot be ruled out. Storchi-Bergmann, Wilson & Baldwin (1996; hereafter SWB96) classified the nuclear spectrum as a LINER, although the details of spatially resolved emission-line profiles and ratios in the inner 2 arcsec have also been interpreted as evidence of a composite spectrum of a Seyfert nucleus and H II regions, as described below. NGC 1672 does not have a 'warm' IRAS colour in the sense of Sanders et al. (1988).

The manifestations of Seyfert activity in the centre of NGC 1672 are the following:

1. Optical spectra of the nucleus of NGC 1672 in a 2×4 arcsec aperture show that its [O III] lines have FWHM ≈ 300 km s^{-1} while its Hβ line has a FWHM of only 150 km s^{-1} (Véron, Véron & Zuiderwijk 1981). These authors argued that the presence of [O III] broader than Hβ is the signature of a composite Seyfert 2/H II region spectrum, in which the [O III] emission comes primarily from a Seyfert nucleus whose [O III]/Hβ ratio is large. The Hβ flux then comes primarily from a region of circumnuclear starburst activity, where there [O III]/Hβ ratio is small (if there is a broad-line region associated with the postulated Seyfert nucleus it must be either intrinsically very weak or obscured; note from Figure 1 the requisite tilted obscuration geometry relative to NGC 1672's disc). Díaz (1985) and García-Vargas et al. (1990) presented spatially resolved spectroscopy of NGC 1672 which shows a strong increase in the [O III] line strength near the nucleus. In the very central region (1.3×1.6 arcsec) [O III]/H$\beta \approx 1$ while away from this region [O III]/Hβ is significantly less than unity. Their spectra reveal that in the very central region both [O III] and Hβ have about the same FWHM of ≈ 300 km s^{-1}. They also show broad wings of Hβ in absorption, the signature of early-type stellar photospheres. All of these feature are present in the nuclear spectra of SWB96 as well, although they classified it as a LINER. Although we have no optical spectra of our own to analyze, we favor slightly the interpretation of Véron et al. (1981) and García-Vargas et al. (1990), who concluded that the spectrum is a composite Seyfert 2/H II region. The LINER classification may simply be an artifact of applying line-ratio diagnostic diagrams to a two-component spectrum.
2. Kawara, Nishida & Gregory (1987) claimed to detect a broad Brackett γ line of atomic hydrogen from NGC 1672 with a width of $1\,100 \pm 380$ km s^{-1}. Their aperture size was 6×3.8 arcsec. In addition, they found that NGC 1672's K band and molecular hydrogen emission suggest that it has an active nucleus (see their sect. III.c). However, Moorwood & Oliva (1988) did not detect the Brackett γ line and set an upper limit on it that is a factor of about two below the detection of Kawara, Nishida & Gregory (1987). Their aperture size was 6×6 arcsec.
3. NGC 1672 has a compact radio source located at its optical nucleus (cf. Plate 2 of Harnett 1987). Lindblad & Jörsäter (1996) recently used the Australia Telescope National Facility to make synthesis maps of the nuclear region, and they find that it is composed of a small nucleus surrounded by an almost circular ring with a radius of about 5.4 arcsec (cf. SWB96; sect. 3 of Sandqvist, Jörsäter & Lindblad 1995). This ring is also seen in Hα, but the correlation between radio and Hα substructure is low. Tovmassian (1968) presented evidence that NGC 1672's 21 cm flux increased by at least a factor of 4 between 1962 and 1965 (there is no further data we know of which examines the claimed variability in more detail). The radio spectral index of Harnett (1987) is 0.73 ± 0.14, typical of optically thin synchrotron emission.

1.3 Previous X-ray observations

NGC 1672 was first detected as an X-ray source by the *Einstein* Observatory (Griffiths et al. 1979; Fabbiano, Feigelson & Zamorani 1982; Fabbiano, Kim & Trinchieri 1992). The 4.9 ks *Einstein* observation yielded 129 ± 16 counts after background subtraction. The X-ray emission was clearly extended but details of the shape were unclear. Crude spectral fitting to a power-law model was performed by Kruper, Urry & Canizares (1990). The observed 0.2–4.0 keV flux was $\approx 7 \times 10^{-13}$ erg cm^{-2} s^{-1}, corresponding to an isotropic luminosity of $\approx 6 \times 10^{40}$ erg s^{-1}.

The GINGA X-ray satellite made both scanning and pointed observations of NGC 1672 on 1991 Aug 3 with the Large Area Counter (LAC) instrument (Awaki & Koyama 1993). A hard X-ray source was seen during the scanning observations in the 0.3×4 degree error box. After background subtraction, the GINGA LAC count rate during the pointed observation was 2.1 count s^{-1} (the pointed observation had an entrance aperture of 1×2 degrees FWHM and no imaging capability within this aperture). The observed 2–10 keV flux was $\approx 3 \times 10^{-12}$ erg cm^{-2} s^{-1}, corresponding to a luminosity of $\approx 2 \times 10^{41}$ erg s^{-1}. The 2–10 keV photon index was measured to be 1.5 ± 0.2 (90 per cent confidence level errors), and the cold column was constrained to be less than 3×10^{22} cm^{-2}. We shall compare the GINGA and *ROSAT* data below.

2 OBSERVATIONS, DATA REDUCTION AND ANALYSIS

ROSAT PSPC (Trümper 1983; Pfeffermann et al. 1987) observations were made of NGC 1672 starting on 1992 Nov 29 (RP701021; total raw exposure of 20.0 ks). *ROSAT* HRI observations were made of NGC 1672 starting on 1992 Jun 24 (RH701022; total raw exposure of 24.4 ks). NGC 1672 was in the centres of the fields of view for both observations. The *ROSAT* observations were performed in the standard 'wobble' mode; to avoid accidental shadowing of sources by the coarse wire grid which forms part of the PSPC entrance window support structure, *ROSAT* performs a slow dithering motion diagonal to the detector axes with a period of ≈ 400 s and an amplitude of 3 arcmin.

Reduction and analysis of the PSPC and HRI data was performed with the Starlink ASTERIX X-ray data processing system.

2.1 Spatial analysis

2.1.1 X-ray sources and naming convention

Figure 1 shows contours of the adaptively smoothed HRI image overlaid on the image from the UK Schmidt

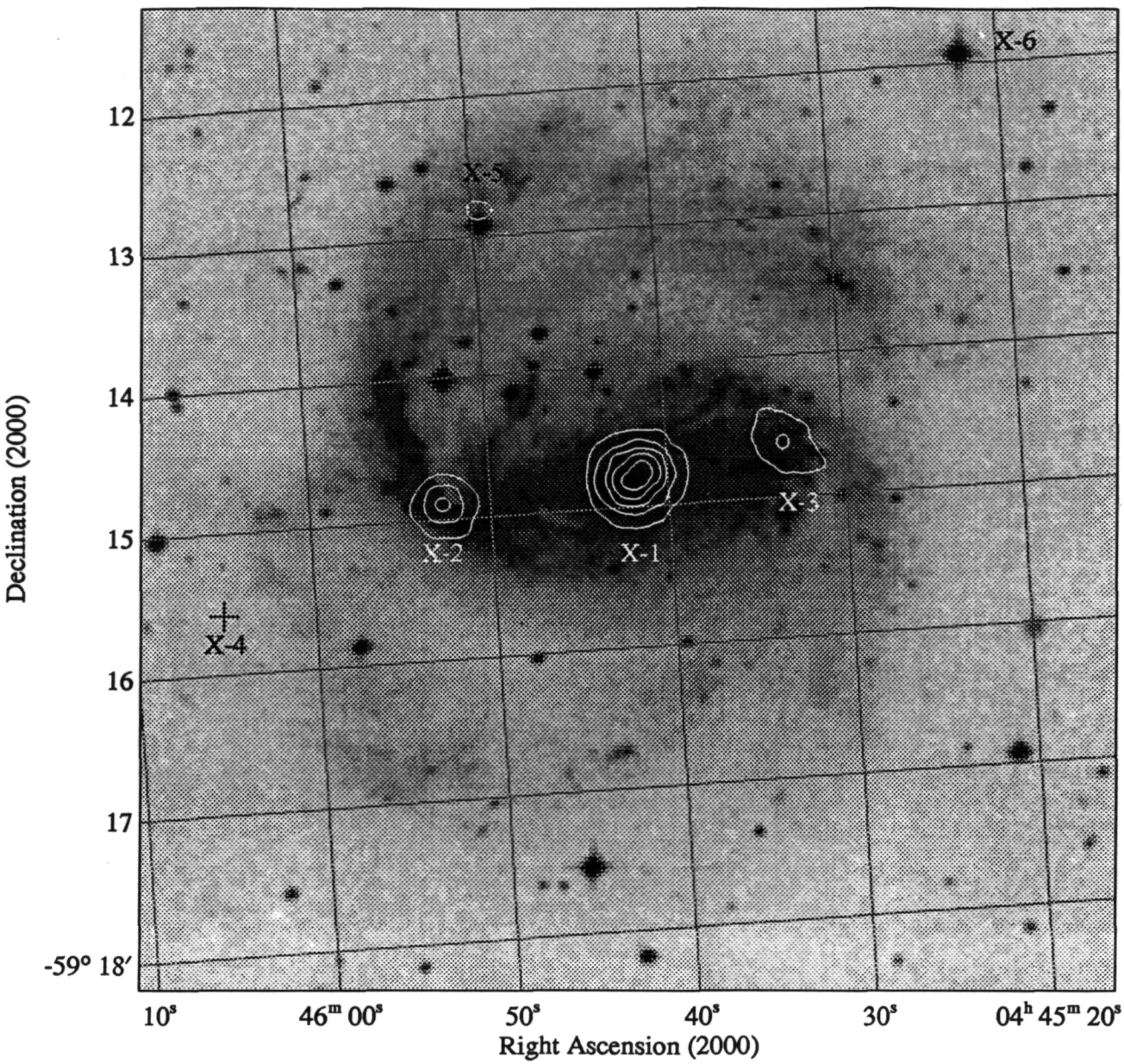

Figure 1. Contours of the adaptively smoothed HRI image overlaid on the image of NGC 1672 from the UK Schmidt southern sky survey J plate. Contours are at 6.4, 11.0, 19.2, 33.5 and 58.2 per cent of the maximum pixel value (see the text for absolute source fluxes). Note the strong central X-ray source and the location of X-ray sources at both end of the bar.

southern sky survey J plate (see sect. IIb of Lasker et al. 1990 for more information on the optical image). The adaptive smoothing algorithm is described in Rangarajan et al. (1995) and Ebeling & White, in preparation. We have set the area that we smooth over by requiring that 25 photons lie within it, and we use a circular tophat smoothing function. Figure 2 shows the adaptively smoothed PSPC image using PSPC channels 50–200. We have set the area that we smooth over by requiring that 10 photons lie within it. In Table 1 we list the positions of X-ray sources detected near NGC 1672 and give their statistical significances and numbers of counts.

NGC 1688 also lies in the field of view of the PSPC observation, but is not detected as an X-ray source. Starburst activity may not have been triggered in NGC 1688 by the putative interaction due to its smaller mass. The smaller galaxy is thought to be the gas loser in most interactions.

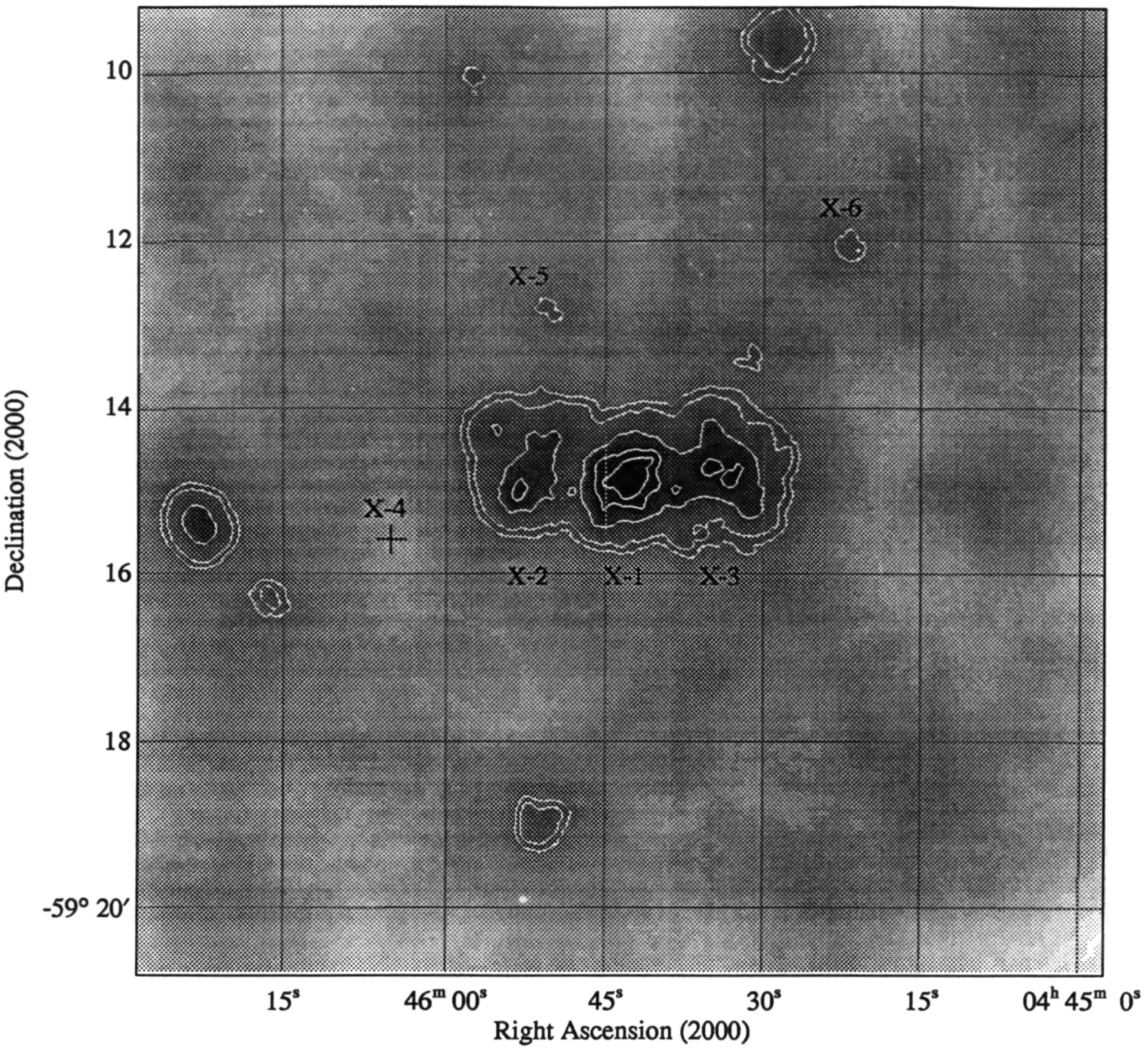

Figure 2. The adaptively smoothed PSPC image of NGC 1672 using PSPC channels 50–200. The shading is logarithmic and contours are at 1.1, 1.6, 5.1, 16.0 and 40.3 per cent of the maximum pixel value (see the text for absolute source fluxes).

2.1.2 Association of the X-ray sources with sources at other wavelengths

The compact radio core of NGC 1672 has a centroid position of α_{2000} = 04h45m42.48s, δ_{2000} = −59d14m50s (Lindblad & Jörsäter 1996), and this agrees with the X-ray centroid position of X-1 to within its error. The centroids of X-2 and X-3 are separated by 2.4 arcmin and lie at the ends of NGC 1672's bar. We also note that in the PSPC image there appears to be some weak emission from a separate pointlike source just to the Northwest of X-3. This emission coincides with an optically bright region along one of NGC 1672's arms (compare Figures 1 and 2).

X-4 is of interest because it lies reasonably close to NGC 1672's centre and because it is fairly firmly detected by the HRI yet not by the PSPC (despite the fact that the PSPC observation is deeper). The second fact suggests potential variability in this source. It lies about 0.5 arcmin off of the main part of one of the arms and there is no matching source on the UK Schmidt image or in NED.

X-5 is located near a bright foreground star which has an optical position of α_{2000} = 04h45m50s, δ_{2000} =

Table 1. X-ray sources near to NGC 1672.

Name	α_{2000}	δ_{2000}	Separation from X-1	HRI counts	HRI Sig.	PSPC counts	PSPC Sig.
	04 45 07.4	−59 20 17.1	7.0	8.0 ± 2.8	3.6	—	—
	04 45 08.2	−59 15 16.7	4.1	7.8 ± 2.8	3.4	5.6 ± 2.4	3.5
	04 45 11.4	−59 12 47.8	4.4	8.0 ± 2.8	3.7	—	—
X-6	04 45 21.7	−59 12 00.0	4.0	14.1 ± 3.8	4.1	7.7 ± 2.7	4.5
	04 45 28.8	−59 09 27.3	5.7	14.0 ± 3.7	4.1	29.5 ± 5.4	8.3
X-3	04 45 33.9	−59 14 40.3	1.1	73.3 ± 8.6	8.0	179.8 ± 13.4	25.1
	04 45 40.6	−59 17 47.9	2.9	7.5 ± 2.7	3.1	5.2 ± 2.3	3.6
X-1	04 45 42.2	−59 14 51.1	0.0	217.5 ± 14.7	26.4	452.5 ± 21.3	51.8
X-5	04 45 49.8	−59 12 48.9	2.3	15.5 ± 3.9	5.4	9.3 ± 3.1	4.1
	04 45 51.2	−59 18 59.9	4.3	—	—	12.1 ± 3.5	5.8
	04 45 51.1	−59 10 52.0	4.0	7.0 ± 2.6	2.9	6.2 ± 2.5	3.2
X-2	04 45 53.2	−59 14 57.8	1.4	62.0 ± 7.9	10.6	117.1 ± 10.8	19.4
	04 45 58.8	−59 10 15.0	5.1	—	—	7.9 ± 2.8	4.0
X-4	04 46 05.1	−59 15 34.8	3.0	12.0 ± 3.4	4.3	—	—
	04 46 16.5	−59 16 14.7	4.6	—	—	15.8 ± 4.0	5.3
	04 46 23.2	−59 15 26.8	5.2	15.0 ± 3.9	5.3	33.3 ± 5.8	11.7

α_{2000} and δ_{2000} give the J2000 X-ray centroid positions as determined with the ASTERIX program PSS. We quote HRI positions whenever possible but when sources are only detected by the PSPC we quote PSPC positions. HRI positions have errors of ≈ 5 arcsec and PSPC positions have errors of ≈ 20 arcsec taking into account boresight and other positional errors. The third column is the separation in arcmin between the centroid of the source and the centroid of source X-1 (which lies in the centre of NGC 1672). HRI counts and PSPC counts are the raw number of counts after background subtraction. When determining the number of counts we use the full HRI band and channels 50–200 (corresponding to 0.5–2.0 keV) of the PSPC band. HRI and PSPC significances are determined using PSS. When determining significances we use the full HRI band and channels 50–200 of the PSPC band. We list all sources that are detected with greater than 3.5σ significance by either the HRI or the PSPC (and we list the significance of the source in the complementary detector as well if this significance is greater than 2.8 sigma).

−59d12m56s. The separation between the optical star and the X-ray centroid is 7 arcsec, and this is the most probable identification for the X-ray source. The star is not listed in SIMBAD and we have not been able to correct its optical position for any proper motion. Similarly, X-6 also appears to be associated with a foreground star.

The other unnamed sources listed in Table 1 do not have any bright optical counterparts. Many of them are probably background sources.

2.1.3 X-ray spatial extents

In Figure 3 we plot HRI radial brightness profiles of X-1, X-2 and X-3. In making this figure, we have conservatively excluded HRI channels 1–3 to avoid any contamination by UV light (cf. sect 3.6 of David et al. 1995). Source X-1 and perhaps source X-3 appear to be extended when compared to the HRI point spread function (PSF; we obtain the PSF from Section 3.2.3 of David et al. 1995 and consider the empirical range of PSFs discussed there). We are aware of the effects the wobble can have on source extensions (cf. Morse 1994), but we are in the fortunate position of having three sources to compare. The fact that X-1 is significantly more extended than X-2 strongly suggests that its apparent extent is real and not an artifact of the wobble. Similarly, the extent of X-3 is also probably real. None of the sources in the HRI field are bright enough to allow us to perform wobble correction using the Morse code HRIASPCOR in FTOOLS.

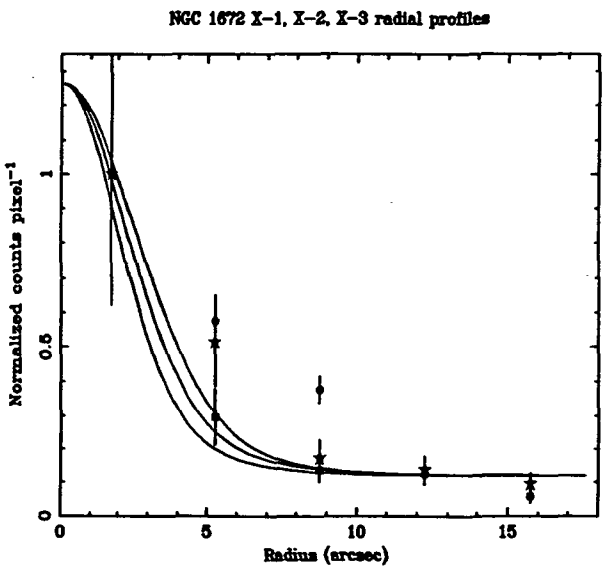

Figure 3. HRI radial profiles of NGC 1672 X-1 (circles), X-2 (squares) and X-3 (stars). Each source's first data point is normalized to unity. The expected range of the HRI PSF from David et al. (1995) is graphed as the three solid curves, shifted so that they asymptotically match the background level.

2.1.4 *Source count extractions for light curves and spectra*

When preparing the light curves and spectra presented below, we have extracted the source counts from carefully chosen source cells that include as many source counts as possible while minimizing cross-source contamination at low energies between X-1, X-2 and X-3. This is difficult in the regions between the sources due to the electronic 'ghost imaging' which widens the point spread function below about 0.3 keV (Hasinger et al. 1992). We discuss this issue in more detail below.

Background counts were subtracted from the source cells using large, nearby circular source-free background cells. Corrections were included for detector dead time, vignetting and shadowing by the coarse mesh window support.

2.2 Temporal analysis

Count rates should be averaged over an integer multiple of the 400 s *ROSAT* wobble period when used for source flux determination (cf. Brinkmann et al. 1994). We do not detect any highly statistically significant variability of X-1, X-2 or X-3 within either the PSPC or the HRI data. When we compare count rates for X-1, X-2 and X-3 using the PIMMS software and the best fitting spectral models described below, there is no strong evidence for variability between the PSPC and HRI observations.

2.3 Spectral analysis

2.3.1 *Relative X-ray energy distributions*

To gain model independent insight into the spectral differences between X-1, X-2 and X-3, we compared their relative X-ray spectral energy distributions (Figure 4). Counts from the corrected PSPC source cells were binned so that one data point in Figure 4 corresponds to 30 PSPC channels, and we have ignored channels below 30 to minimize cross-source contamination. Note that X-1 is the softest of the three sources while X-3 is the hardest.

2.3.2 *Binning and calibration of source spectra*

For our spectral fitting, counts from the corrected PSPC source cells were binned into 256-channel, pulse-invariant spectra. We ignored channels 1–8 and rebinned the extracted spectra so that at least 20 source photons were present in each bin.

Systematic errors of 2 per cent were added in quadrature to the data point rms errors to account for residual uncertainties in the spectral calibration of the PSPC. We have used the 1993 January response matrix. It corrects for the systematic deficit of photons near the carbon edge of the PSPC detector that was present in earlier matrices (cf. Turner, George & Mushotzky 1993). The expected systematic errors from this matrix are a few per cent.

2.3.3 *Spectral fitting preliminaries and information about neutral hydrogen column*

We model the X-ray spectra presented below using the spectral models in the XSPEC fitting package (Shafer et al. 1991).

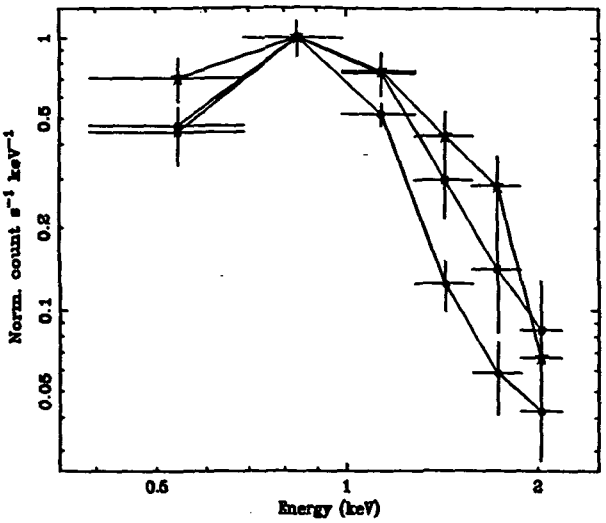

Figure 4. PSPC spectra of NGC 1672 X-1 (circles), X-2 (squares) and X-3 (stars). These spectra have been normalized so that their maxima correspond to unity. Note the relative numbers of hard counts from each source.

The errors for all fits shall be quoted for 90 per cent confidence (unless explicitly stated otherwise), taking all free parameters to be of interest other than absolute normalization (Lampton, Margon & Bowyer 1976; Press et al. 1989).

Due to the southerly declination of NGC 1672, its Galactic neutral hydrogen column density is not given in any of the 21 cm catalogs. Fabbiano et al. (1989) adopted a Galactic column of $N_{\rm H} = 3.0 \times 10^{20}$ cm^{-2} to NGC 1672 because of its high Galactic latitute ($-39°$).

The nuclear region of NGC 1672 has a large Balmer decrement of $H\alpha/H\beta \approx 10$, which OSW74 argue is caused by dust reddening in NGC 1672 with $E(B-V) \approx 1.3$. If we assume a 'Galactic' dust-to-cold-gas ratio, the corresponding neutral hydrogen column density is $N_{\rm H} \approx 7 \times 10^{21}$ cm^{-2} (cf. sect. VI of Burstein & Heiles 1978). However, SWB96 argue that the Balmer emission lines need to be corrected for the underlying absorption lines of the early stellar population, which affects $H\beta$ more strongly than $H\alpha$. After subtracting an appropriate stellar template spectrum, the resulting Balmer decrement at the nucleus corresponds to $E(B-V) \approx 0.16$, or $N_{\rm H} \approx 9 \times 10^{20}$ cm^{-2}. However, $E(B-V)$ values of 0.4–0.6 are seen within the spatial region corresponding to X-1. Interestingly, the derived extinction is smaller in the nucleus than in regions of surrounding star formation, in which $E(B-V)$ as large as 0.7 is seen (see Table 9 of SWB96).

Despite its large Balmer decrement and significantly reddened UV continuum, the *IUE* spectrum of NGC 1672 (Kinney et al. 1993) shows no evidence of the 2175 Å dust absorption feature often associated with small graphite grains (e.g. sect. 1.4 of Tielens & Allamandola 1987; sect. 2.1.2 of Mathis 1990). This peculiar effect has been seen in many star forming galaxies (sect. 4.2.4 of Kinney et al. 1993; Calzetti, Kinney & Storchi-Bergmann 1994). It may suggest either an unusual dust chemical composition/grain size distribution or clumpy dust that acts as a 'picket fence' (we discuss and examine these possibilities below). The

weakness of the 2175 Å feature in parts of the LMC and SMC is often attributed to their low metallicities (e.g. sect. 45.5 of Lequeux 1988). There is also evidence that the carriers of the 2175 Å feature are very sensitive to the strength of the local radiation field (Leene & Cox 1987; Rosa & Benvenuti 1995). The depth of the absorption feature decreases as the radiation field gets stronger, perhaps due to the destruction of the carrier particles.

In the following sections, we shall refer to dust that lacks the carrier of the 2175 Å feature (either due to a peculiar chemical composition or grain size distribution) as CDD ('carrier deficient dust').

2.3.4 Spectral fitting to NGC 1672 X-1

The *ROSAT* PSPC spectrum of X-1 is shown in Figure 5. To avoid confusion by cross-source contamination, we fit only the data above PSPC channel 30 where X-1, X-2 and X-3 are fairly cleanly separated. A power-law model, as might be expected if electron scattered X-ray emission from a Seyfert nucleus dominated the spectrum, is statistically unacceptable ($\chi^2_\nu = 2.0$) and gives an unphysically steep photon index ($\Gamma > 10$). This is understandable due to the very steep drop-off in X-ray flux above ≈ 1 keV. If we fit only the data above PSPC channel 50, a simple power-law model can still be ruled out with greater than 95 per cent confidence unless its photon index is greater than 6.0. Such a steep soft X-ray spectrum is never seen Seyfert galaxies and thus a simple power-law model for X-1 is unphysical. The residuals suggest that a power-law fit is poor due to the robust overall shape of the spectrum and not due to just a few stray data points. Deleting sets of points confirms this conclusion.

Electron scattering mirrors in which the atoms in the mirror are not fully stripped of their electrons can also imprint X-ray emission lines on a scattered X-ray spectrum. The strongest such emission lines in the *ROSAT* band are from iron L. We consider an electron scattering mirror that imprints iron L lines by fitting our data to an absorbed power-law model with a Gaussian emission line. The centroid energy of the line is chosen to lie in the range 0.85–1.0 keV, and the line width (σ) is chosen to lie in the range 0.05–0.20 keV (this is a reasonable model for the iron L complex given the limited spectral resolution of *ROSAT* and the small number of counts in our spectrum). While some choices of line parameters in these ranges give statistically acceptable fits, the underlying photon indices derived from such fits are always significantly larger (> 2.5) than are seen in Seyfert 2 galaxies (the soft X-ray spectra of Seyfert 2's are flattened in scattering and have photon indices in the range 1.0–1.6). In addition, the iron L complex equivalent widths derived from our fitting are always larger than 700 eV (and flatter spectra tend to require larger iron L complex equivalent widths). Such equivalent widths, while not impossible, are large compared to what is seen in, for example, Mrk 3 (Iwasawa et al. 1994).

Simple absorbed bremsstrahlung and blackbody models are poor fits to the data and can be rejected with > 99 and > 95 per cent confidence, respectively. They both leave large systematic residuals in the 0.7–1.0 keV range.

Massive or low-mass X-ray binary sources similar to those in the Milky Way are not likely to make major contributions to X-1's *ROSAT* band X-ray flux due to its soft spectrum and fairly steep X-ray drop-off above ≈ 1 keV (cf. sect. III.b of Fabbiano 1988; sect. 4.2 of David, Jones & Forman 1992). They may, of course, contribute significantly at higher energies. Some contribution from 'supersoft' X-ray binaries to the *ROSAT* flux may be possible.

A Raymond-Smith thermal plasma model with cold absorption gives a good fit with $N_{\rm H} = (1.6^{+2.4}_{-1.6}) \times 10^{20}$ cm^{-2}, $kT = 0.68^{+0.15}_{-0.08}$ keV and $\chi^2_\nu = 0.7$. The quality of the thermal plasma fit, the arguments above regarding scattered X-ray emission, and the significant spatial extent of X-1 suggest that the starburst activity in NGC 1672 dominates its X-ray emission along our line of sight (although we cannot rigorously rule out a substantial contribution of scattered X-rays from a Seyfert nucleus). The derived metal abundance by number relative to the cosmic one (Anders & Grevesse 1989) is $0.12^{+0.40}_{-0.08}$. Such a low derived abundance in the centre of a spiral galaxy appears surprising, and such a low abundance is not suggested by observations at other wavelengths (e.g. Alloin et al. 1979; Storchi-Bergmann, Calzetti & Kinney 1994; SWB96). It must be remembered, however, that due to our limited number of counts we only fitted a single temperature plasma model to what is probably emission from a multiple temperature plasma. This simplification can confuse abundance determinations. Fits with two solar-abundance Raymond-Smith plasmas are statistically acceptable and physically reasonable, albeit poorly constrained by our data. In addition, scattered X-rays from the Seyfert nucleus could further complicate the spectrum (although as explained above we suspect they do not dominate it). Fluxes and the isotropic luminosity of X-1 are given in Table 2.

The fitted cold hydrogen column is consistent with what we expect for the Galactic column, and we do not see evidence for absorption by gas associated with the large amounts of dust discussed by OSW74. This remains true even if we fix the abundance at the cosmic one (or several times it). Multi-component models, which include an additional thermal plasma or power-law component, do not facilitate the presence of a neutral column as large as would be expected based on OSW74. If we fix the column at $N_{\rm H} = 7 \times 10^{21}$ cm^{-2} (see the previous section for why we choose this value), we are not able to obtain statistically acceptable fits even with complicated spectral models (the fits are always poor below 0.5 keV). The same is true even if we lower the column to $N_{\rm H} = 3 \times 10^{21}$ cm^{-2}. A column of $N_{\rm H} = 9 \times 10^{20}$ cm^{-2} (again see the previous section) can be statistically accomodated by multi-component model fits, although the best fitting multi-component models generally have columns of $< 5 \times 10^{20}$ cm^{-2}. We shall discuss the absorption of the nuclear source in more detail below.

If we include the data points below 0.3 keV in our fitting, our results are not significantly changed from those above.

2.3.5 Spectral fitting to NGC 1672 X-2 and X-3

We shall again use only the data above PSPC channel 30 to prevent cross-source contamination. Due to the small numbers of counts from X-2 and X-3, our spectral models are not tightly constrained, and we shall quote 68.3 per cent confidence errors throughout this section.

A simple absorbed power-law model for X-2's spec-

Table 2. Raymond-Smith thermal plasma models of X-ray sources in NGC 1672.

Quantity	Source X-1	Source X-2	Source X-3
χ^2_ν	0.7	0.7	0.6
kT (keV)	$0.68^{+0.15}_{-0.08}$	$1.1^{+1.2}_{-0.3}$	$1.7^{+1.3}_{-0.6}$
Abundance ⋆	$0.12^{+0.40}_{-0.08}$	< 0.26	< 0.38
$N_{\rm H}/(1 \times 10^{20}$ cm$^{-2})$	$1.6^{+2.4}_{-1.6}$	3.0†	3.0†
(0.1–2.5 keV Absorbed $F_{\rm X}$)$/(1 \times 10^{-13}$ erg cm^{-2} s^{-1})	2.6	0.87	1.1
(0.1–2.5 keV Unabsorbed $F_{\rm X}$)$/(1 \times 10^{-13}$ erg cm^{-2} s^{-1})	3.6	1.3	1.5
(0.1–2.5 keV $L_{\rm X}$)$/(1 \times 10^{40}$ erg s^{-1})	2.1	0.76	0.88
$EM/(1 \times 10^{63}$ cm$^{-3})$	2.2	1.2	1.0
n (cm^{-3})	> 0.17	> 0.36	> 0.17
M (M$_\odot$)	$< 1.1 \times 10^7$	$< 2.8 \times 10^6$	$< 4.8 \times 10^6$
E (erg)	$< 1.4 \times 10^{55}$	$< 5.8 \times 10^{54}$	$< 1.6 \times 10^{55}$
P (dyne cm^{-2})	$> 3.8 \times 10^{-10}$	$> 1.3 \times 10^{-9}$	$> 9.6 \times 10^{-10}$

We quote 90 per cent errors for X-1 and 68 per cent errors for X-2 and X-3. EM is the emission measure, calculated as is described in the 'Raymond' model description of Shafer et al. (1991). n is the mean emitting gas density averaged over the source, M is the mass of the emitting gas, E is the thermal energy content of the emitting gas and P is the pressure of the emitting gas. Our calculations of n, M, E and P parallel those given in sect. 4.1 of Armus et al. (1995), and we have assumed homogeneous spherical emission regions. We take the radial extent of X-1 to be less than 8 arcsec, which corresponds to 880 pc; the radial extent of X-2 to be less than 4 arcsec, which corresponds to 440 pc; and the radial extent of X-3 to be less than 6 arcsec, which corresponds to 660 pc (see Figure 3).

⋆ Note that the ROSAT fit abundances are probably not physically meaningful; see the text.

† Column fixed at this value (see the text).

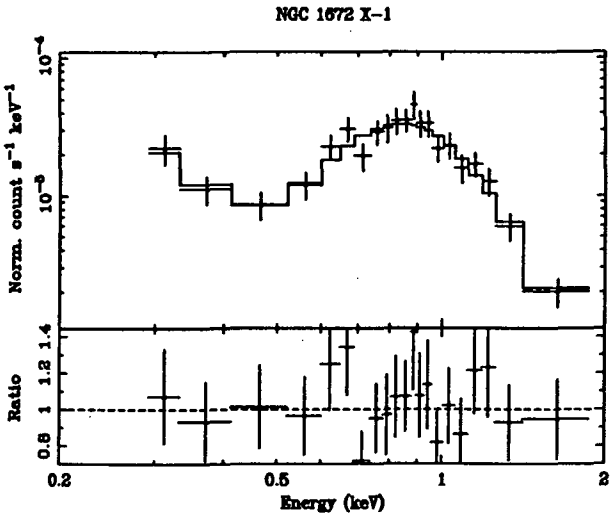

Figure 5. PSPC spectrum of NGC 1672 X-1. A Raymond-Smith thermal plasma model with cold absorption is also shown with the corresponding data-to-model ratio.

trum gives $\Gamma = 2.6^{+2.0}_{-0.8}$, is consistent with the Galactic column, and cannot be ruled out on statistical grounds (it has $\chi^2_\nu = 0.7$). However, given the starburst nature of X-2's location, we suspect that an absorbed Raymond-Smith thermal plasma model may be more appropriate. Using this model we obtain $N_{\rm H} = (3.9^{+24}_{-3.9}) \times 10^{20}$ cm^{-2}, $kT = 1.0^{+5.1}_{-0.7}$ keV and $\chi^2_\nu = 0.9$ (the associated abundance is not well constrained). In the above fitting the parameters are loosely constrained due to the fact that the neutral hydrogen column can become very high. If we assume there is no significant intrinsic hydrogen column and fix the column at $N_{\rm H} = 3.0 \times 10^{20}$ cm^{-2} (this is at least plausible for NGC 1672's inclination and our results for X-1), we obtain $kT = 1.1^{+1.2}_{-0.3}$ keV and $\chi^2_\nu = 0.7$. The associated abundance is constrained to be less than 26 per cent of the cosmic value (but see the important caveats in the previous section). Fluxes and the isotropic luminosity of X-2 may be found in Table 2.

A simple absorbed power-law model for X-3's spectrum gives $\Gamma = 2.0^{+1.2}_{-0.7}$, is consistent with the Galactic column, and cannot be ruled out on statistical grounds (it has $\chi^2_\nu = 0.6$). As per X-2, however, we suspect that an absorbed Raymond-Smith thermal plasma model may be more appropriate. Using this model we obtain $N_{\rm H} = (2.5^{+11}_{-2.5}) \times 10^{20}$ cm^{-2}, $kT = 1.8^{+5.0}_{-0.8}$ keV and $\chi^2_\nu = 0.7$ (the associated abundance is not well constrained). If, as per the previous paragraph, we fix the column at $N_{\rm H} = 3.0 \times 10^{20}$ cm^{-2}, we obtain $kT = 1.7^{+1.3}_{-0.6}$ keV and $\chi^2_\nu = 0.6$. The associated abundance in constrained to be less than 38 per cent of the cosmic value. Fluxes and the isotropic luminosity of X-3 may be found in Table 2.

2.3.6 Comparison of ROSAT and GINGA spectral results

Using the GINGA spectral parameters given in Sect. 1 and the *ROSAT* spectral parameters and data described above, we have compared the spectra from these two satellites. If the GINGA spectral data were dominated by a central active nucleus in NGC 1672 and the flux from this nucleus did not vary with time, then one would expect the low-energy end of the GINGA spectral model to join fairly smoothly

onto the high-energy end of the *ROSAT* PSPC X-1 spectrum. This is not observed. Instead the low-energy end of the GINGA spectral model is a factor of ≈ 7 times higher than the high-energy end of the *ROSAT* PSPC spectrum of X-1, even when the upper limit on the column given by Awaki & Koyama (1993) is used. This suggests that either the GINGA spectral data were not dominated by a central active nucleus in NGC 1672 (at least at the low-energy end of the GINGA band) or the hard X-ray flux from the central nucleus decreased between the GINGA (1991 Aug 3) and *ROSAT* (1992 Nov 29) observations. We cannot rule out hard X-ray variability, and such variability may be probed for with future observations. Obvious additional contributors to the GINGA spectrum could be X-ray binaries in X-2 and X-3. If we create a *ROSAT* spectrum that includes all the emission from X-1, X-2 and X-3, then the agreement between the GINGA and *ROSAT* data is significantly improved (even though X-2 and X-3 are weaker overall than X-1, note from Fig. 4 that they are harder). The mismatch between the low-energy end of the GINGA spectral model and the high-energy end of the *ROSAT* data is only a factor of ≈ 2. If, as our analysis suggests, X-2 and X-3 contribute to the GINGA flux, then the true column density to the nuclear source is probably larger than the upper limit that GINGA measured. Of course, sources external to NGC 1672 could also contribute to the GINGA flux. Our *ROSAT* field does not have any sources that are much stronger than NGC 1672 in it, but there are four sources of roughly comparable soft X-ray flux that could contribute hard flux.

3 DISCUSSION

3.1 Source X-1

3.1.1 Optical, UV and X-ray absorption

Our *ROSAT* spectrum constrains the *flux-weighted* average amount of neutral gas (both in atomic and molecular form) along our lines of sight to the X-ray sources in the nuclear region. The fact that we do not see a large cold column associated with the nuclear region (from our fitting to X-1), combined with its other absorption properties (optical reddening, UV continuum reddening, lack of 2175 Å feature; see sect. 2.3.3), suggests either peculiar absorption physics or an interesting source geometry. We shall adopt the optical reddening analysis of TWB96 rather than that of OSW74.

In this paragraph we examine how/whether peculiar absorption physics might explain the optical, UV and X-ray absorption properties. We shall make the assumption that the optical, UV and X-ray emissions all traverse a screen of matter between their sources and Earth (we shall then examine the case when this assumption is false). Cold gas associated with the CDD described Sect 2.3.3 might explain the X-ray data if the X-ray spectrum has multiple components. A somewhat larger than 'Galactic' dust-to-cold-gas ratio is suggested, however. If the some of the gas associated with the dust were ionized (so that it did not contribute to the cold X-ray column), this could explain the higher suggested value of this ratio. Another possible type of screen that could be traversed by the optical, UV and X-ray emissions on their way to Earth is one that consists of thick clumps of dust along the line of sight ('picket fence' dust as discussed in sect. 4.2.4 of Kinney et al. 1993; hereafter PFD). PFD might explain the lack of the 2175 Å feature if the dust clumps were opaque to the UV and thus just lowered the detected UV flux without changing the UV spectral shape (i.e. imprinting the 2175 Å feature). However, such clumps then have difficulty explaining the large Balmer decrement and the reddened UV continuum. Thus a PFD model for the nuclear region's absorption seems to be untenable.

Now we examine how/whether source geometry might explain the optical, UV and X-ray absorption properties. We shall not make the assumption that the optical, UV and X-ray emissions all traverse an absorbing screen between their sources and Earth. Because the X-ray fits to X-1 provide a *flux-weighted* average measure of the amount of neutral gas between us and the X-ray sources in the nuclear region, heavily absorbed sources that are faint as a result of absorption by neutral gas will contribute less to this average than similar sources that are not heavily absorbed (cf. sect. 1 of Witt, Thronson & Capuano 1992). Thus, the true average amount of absorbing gas present might be underestimated by the fitted cold X-ray column. Similar considerations apply to the optical and UV emissions. In light of this argument, a model to explain the absorption properties of the nuclear region might involve some sources that are heavily obscured and some that are not (along the lines of what is discussed in sect. 3.6 of Calzetti, Kinney & Storchi-Bergmann 1994). The heavily obscured sources would produce the large observed *nebular* Balmer decrement, while the sources that are not heavily obscured would not contribute significantly to the Balmer lines since they lack the requisite nebulae. The sources that are not heavily obscured would dominate the optical continuum, the ultraviolet continuum longward of 1200 Å (hence diluting away any 2175 Å feature), and the soft X-ray continuum (hence leading to the low $N_{\rm H}$ fit value).

Another geometrical way to explain the optical, UV and X-ray absorption properties would be to locate the optical and UV sources behind a CDD screen as above, but not the X-ray emitting sources. Such a situation might be realized if X-ray emitting gas were expelled to a position outside or above the screen, perhaps by a superbubble or superwind. A point in favour of this general idea is the erratic behaviour of the [O III] lines near the nucleus. As noted by Lindblad & Jörsäter (1996), large velocity jumps and changes of shape occur over distances of an arcsec. These authors speculate that this behaviour is due to an outflow directed close to the line of sight. This is in line with what might be expected for a starburst superwind, and if a superwind deposited gas above the plane of NGC 1672 this could explain the small X-ray column that we measure. The spatial extents of X-1 and X-3 appear to be larger than the ~ 150 pc scale height of a typical galactic interstellar medium, and this fact also suggests that a significant amount of X-ray emitting gas may lie above the starburst region (which is probably confined to about the height of the molecular cloud layer).

3.1.2 Comparison with other wavelengths and the origin of the soft X-ray emission

The soft X-ray isotropic luminosity we derive for X-1 is only a small fraction of the total isotropic luminosity of NGC 1672's central region. In the near-infrared the K-band nu-

clear isotropic luminosity in a 3 arcsec diameter aperture is 1.0×10^{42} erg s^{-1} (Forbes et al. 1992), and significant extended emission is seen as well. In the far-infrared, NGC 1672 has a 40–120 μm isotropic luminosity of 9.6×10^{43} erg s^{-1} (Maia et al. 1994 corrected to $H_0 = 50$ km s^{-1} Mpc^{-1}).

The 5000 MHz (6 cm) radio luminosity of NGC 1672 is 3.2×10^{38} erg s^{-1}. Comparison of our spatially resolved X-ray maps and Plate 2 of Harnett (1987) is revealing. It shows that despite the fact that X-1 is only stronger than X-2 or X-3 by a factor of ≈ 2.5, the central region is at least 15 times more powerful than the regions near X-2 and X-3 at 843 MHz (36 cm). The fact that the central region is $\gtrsim 6$ times more efficient at producing 843 MHz radio flux per unit X-ray flux immediately suggests that either (1) the energy generation mechanism in the central region is different from those near X-2 and X-3 or (2) there is an additional producer of radio flux associated with the central region that does not generate large amounts of X-ray flux. Although our constraints on the best-fit X-ray specta of X-2 and X-3 are not tight, their spectra do not appear to be strongly different from that of X-1 (although they are somewhat harder), suggesting that the X-ray generation mechanisms may not be strongly dissimilar. The spectral luminosity of NGC 1672 at 1410 MHz (21 cm) is 2.4×10^{22} W Hz^{-1}. Comparison with fig. 4 of Ulvestad & Wilson (1984) shows that this is a fairly typical 1410 MHz spectral luminosity for a Seyfert nucleus, although comparison with fig. 1 of Davies (1989) shows that it is not entirely out of the range of 'normal' spirals.

Using a 20 arcsec aperture, OSW74 measured an uncorrected Hβ isotropic luminosity from NGC 1672 of 1.6×10^{40} erg s^{-1} (we correct to the distance of Sect. 1.1). After correcting for their $E(B-V) = 1.3$, they infer a true Hβ isotropic luminosity of 1.1×10^{42} erg s^{-1}. They also pointed out that the appropriate correction could be even larger than this if internal dust is present. However, if we adopt a smaller average $E(B-V)$ of $\simeq 0.5$ from the starlight-subtracted, near-nuclear measurements of SWB96, then the intrinsic Hβ luminosity is only increased to 8×10^{40} erg s^{-1}. The true value is perhaps somewhere between these extremes. The Lyman continuum photon number derived by OSW74 from their corrected Hβ isotropic luminosity is 1.7×10^{54} photons s^{-1}. Ward (1988) used the Brackett γ data of Kawara, Nishida & Gregory (1987) to derive an ionizing photon number of 1.1×10^{53} photons s^{-1} (we correct to the distance of Sect. 1.1). The latter estimate is much less dependent on the correction for dust absorption than the estimate of OSW74 (although none has been made), and is derived using a smaller aperture size of 6×3.8 arcsec. Given the size of the nuclear region in NGC 1672, the discrepancy of a factor of ≈ 9 between these two measurements might be partly due to the different aperture sizes. In addition, however, it probably supports the lower extinction estimates of SWB96. Thus the calculation of Ward (1988) is in general agreement with Balmer-line measurements in the nuclear region of NGC 1672, although the data of Moorwood & Oliva (1988) show that any conclusions drawn from the Brackett γ data on NGC 1672 of Kawara, Nishida & Gregory (1987) must be treated with caution. Based on their Lyman photon counting, OSW74 suggested that about 160 000 ionizing stars are present in the nuclear region, together with the rest of a young stellar population. The extinction values of SWB96, on the other hand, argue that the true number is probably a factor of about 10 smaller.

The Lyman continuum photon number of Ward (1988) is ~ 11 times larger than that from the R136 nebula of 30 Doradus ($\gtrsim 10^{52}$ photons s^{-1}; Wang & Helfand 1991), the most luminous H II region in the Local Group. If we assume identical stellar-type distribution functions for the central region of NGC 1672 and the R136 nebula, the number of ionizing stars in the central region of NGC 1672 will be ~ 11 times larger than that in the R136 nebula. If we scale the soft X-ray luminosity of the R136 nebula ($(1\text{–}4)\times 10^{37}$ erg s^{-1}; Wang & Helfand 1991) by this factor, we derive a characteristic soft X-ray luminosity of only $(1\text{–}4.4)\times 10^{38}$ erg s^{-1}. This is to be compared with X-1's isotropic luminosity in soft X-rays of 2×10^{40} erg s^{-1}. Even if we adopt the larger Lyman continuum flux of OSW74, we can only account for $(2\text{–}7)\times 10^{39}$ erg s^{-1} by analogy with R136. Hence the nuclear activity in the central region appears to be more efficient in generating X-rays per Lyman continuum photon than the activity in R136, perhaps due to a larger fractional contribution from non-stellar processes such as supernovae, or heating by a hidden Seyfert 1 nucleus.

It is unlikely that O stars directly produce most of X-1's X-rays. For a typical O star luminosity of 5×10^{33} erg s^{-1} (cf. Harnden et al. 1979), about four million O stars would be required. However, most of the X-rays associated with O stars do not come directly from the stars themselves but instead from the energy that their winds and supernovae deposit in the interstellar medium. Following the argumentation in sect. 3.2 of Wang & Helfand (1991) and taking into account the ≈ 8 Myr age (Díaz 1985), it is energetically possible that X-1 arises from a violent interstellar medium similar to that seen in R136 but on a much larger scale. Stellar winds carve out hot cavities in the neutral interstellar medium and subsequent supernovae occur in hot, low-density environments where they do not form bright remnants but do heat the hot component of the interstellar medium. Our X-ray spectral fitting results are in reasonable agreement with this interpretation. The Raymond-Smith temperature of $7.0\text{–}9.6\times 10^6$ K is not dissimilar to the $\approx 6 \times 10^6$ K Raymond-Smith temperature of R136. We have considered contributions to the soft X-ray spectrum from X-ray binaries in Sect. 2.3.4.

In Table 2 we present emission measures for our thermal plasma fits as well as quantities we estimate from these emission measures. The thermal plasma models for X-1, X-2 and X-3 imply surprisingly large densities and thermal energy contents. Because the apparent radius of each source is relatively small, we are forced to consider particle densities of order 0.2 and larger. X-1, X-2 and X-3 contain energies corresponding to about 10^3–10^4 supernovae. Although the sizes and temperatures of these regions are comparable to those expected for superbubbles blown by this many supernovae over a 10^7 yr period (MacLow & McCray 1988, hereafter MM88), their inferred internal densities are much greater, even when the evaporation of the cold dense shell to the interior is included (see eqn. 5 of MM88). The internal pressure of X-1 corresponds to 140 times that of the nearby hot ISM (Bowyer et al. 1995; note that X-2 and X-3 have even higher pressures than X-1). The ambient density required by eqn. 5 of MM88 is ~ 300 cm^{-3}, much higher than the average value that would be expected over an extent of > 440 pc in a spiral galaxy. The amount of mass swept out

of X-1 would be $\sim 10^{10}$ $M_\odot$, an implausible amount. Another argument against such large ambient densities is the absence of X-ray absorption by the correspondingly dense HI supershells which would surround the superbubbles.

What aspect of this scenario could be altered to retain a plausible thermal plasma model? First, the derived emission measures might be overestimates if the fitted abundances are in error. It is difficult, if not impossible, to measure abundances reliably using *ROSAT* data. If the actual metal abundances were the solar ones, for example, then we estimate with XSPEC that the derived emission measure of X-1 could be lower by a factor of about 6. The same argument applies to X-2 and X-3. Indeed, SWB96 derived abundances that are slightly higher than solar in the nuclear region of NGC 1672, and approximately solar along the bar. However, since the average number density only scales as the square root of the emission measure it is hard to imagine that the density could be reduced by more than a factor of four with such a correction. Second, if the hot medium were clumped as a result of the supernova explosions taking place among a large number of giant molecular clouds which have been completely shocked, but have not finished expanding, then the required mass and energy content would be reduced since they scale as the filling factor to the one half power (see sect. 4.1 of Armus et al. 1995; the filling factor is less than unity). Together, these two effects may render plausible a model in which one or more of the main X-ray sources in NGC 1672 are extremely luminous examples of superbubbles of the type envisioned by MM88, and thought to be seen by *ROSAT* in NGC 5408 (Fabian & Ward 1993), NGC 2146 (Armus et al. 1995) and NGC 1569 (Heckman et al. 1995).

Alternatively, for the nuclear source X-1 we may consider a contribution due to photoionization heating by a hidden Seyfert nucleus. Adopting the fitted thermal plasma model as a first approximation, the emission measure is considerably smaller than that of extended X-ray sources in other Seyfert galaxies. For example, the X-ray emission extended over the inner 6 kpc radius in NGC 1068 requires emission measure $\sim 7 \times 10^{64}$ cm^{-3} and electron density $n \sim 0.15$ at an assumed temperature of 10^7 K (Halpern 1992). This medium would be in rough pressure balance with the 'diffuse ionized medium' seen in [N II] and Hα (Bland-Hawthorn, Sokolowski & Cecil 1991). Similarly, Wilson et al. (1992) argued that $(4\text{–}9)\times 10^7$ $M_\odot$ of hot gas would be required to account for the extended *nuclear* X-rays in NGC 1068. In NGC 4151 (Morse et al. 1995), the extended X-ray emission has a luminosity of $\sim 1.7 \times 10^{41}$ erg s^{-1}, which would require a medium of $T \sim 10^7$ K and $n \sim 0.3$ if it were to be in pressure equilibrium with the extended narrow-line region clouds. Both NGC 1068 and NGC 4151 have luminous enough ionizing continua to heat their gas to 10^7 K and render it optically thin to 1 keV X-rays. The required ionization parameter $\xi = L/nr^2$ is ~ 100 for a $\Gamma = 2$ power law. For the case of NGC 1672, taking $n = 0.17$ and $r = 880$ pc requires an ionizing luminosity $L \sim 1 \times 10^{44}$ ergs s^{-1}. This would be a fairly strong Seyfert, and its ionizing luminosity would be comparable to its far-infrared luminosity, although its IRAS *colours* show no evidence for a luminous Seyfert component.

The required intrinsic X-ray luminosity in the Seyfert scenario is about 500 times larger than the 2–10 keV luminosity observed by GINGA, and suggests that if a Seyfert is photoionizing the central region, we are seeing little if any scattered X-ray flux from the nucleus. The properties of X-1 listed in Table 2 allow it to have a Thomson depth of only $\sim 3\times 10^{-4}$, which is not great enough to account for the flux observed by GINGA, although it is roughly compatible with the *soft* X-ray flux being scattered. For either scattering or photoionization heating to account for X-1, the geometry would have to be such as to hide the broad-line region, if any, and the continuum source, but with a relatively large opening angle so as to cause little azimuthal asymmetry in the extended X-ray source, and little reprocessed, warm infrared emission. The existence Seyfert 2 galaxies whose observed X-ray luminosity is even less than 10^{40} erg s^{-1} can perhaps be similarly explained by the lack of a suitable scattering mirror.

3.2 Sources X-2 and X-3

Sources X-2 and X-3 have not been the subjects of detailed studies in the past. Baumgart & Peterson (1986) commented upon vigorous star formation at the ends of NGC 1672's bar seen in near-infrared photographic plates, but did not present quantitative information. Similarly, Hα hotspots at the ends of the bar, as well as along two of the four arms, can be seen in fig. 3 of Sérsic & Calderón (1979), and fig. 2c of SWB96. The abundances seem to be about solar in these regions, and the extinction is $E(B\text{–}V) \approx 0.27$ for both (SWB96). X-2 and X-3 are each over 200 times more luminous in soft X-rays than the R136 nebula of 30 Doradus. Their emission can be modelled by thermal gas emission, although due to their faintness we cannot rigorously rule out a substantial contribution from X-ray binaries.

3.3 An examination of the NGC 1672/NGC 1688 interaction scenario

The 39 arcmin angular separation between NGC 1672 and NGC 1688 corresponds to a separation in the plane of the sky of $\approx$ 260 kiloparsecs. The difference in radial velocities between NGC 1672 and NGC 1688 is about 72 km s^{-1} (Elmegreen et al. 1991). The characteristic separation velocity in the plane of the sky is probably somewhat larger than the radial velocity difference due to geometrical effects (the radial velocities are only one dimensional). In addition, given that a NGC 1672/NGC 1688 interaction took place, the orbital speed will have been larger when NGC 1672 and NGC 1688 were closer together. We estimate that a putative interaction would have happened on the order of 1.5 billion years ago. Since Galactic bars are thought to form on timescales shorter than 1.5 billion years (a few times 10^8 years), this strongly suggests that the starburst activity we see in NGC 1672 is not a direct result of the NGC 1672/NGC 1688 interaction but is rather a more transitory and indirect phenomenon resulting from the nature of the gas flow in the bar.

ACKNOWLEDGMENTS

We acknowledge discussions with D. Calzetti, H. Ebeling, A.C. Fabian, S. Sigurdsson, E. Terlevich, R. Terlevich, M.

Ward and the members of the Institute of Astronomy X-ray group. We thank P.O. Lindblad and S. Jörsäter for kindly sharing some of their results prior to publication. We acknowledge financial support from the United States National Science Foundation and the British Overseas Research Studentship Programme (WNB), NASA grant NAG 5-1935 (JPH) and the JSPC and the British Council (KI). The *ROSAT* project is supported by the Bundesministerium für Forschung und Technologie (BMFT) and the Max-Planck society. Much of our analysis has relied on the ASTERIX and FTOOLS X-ray data processing systems and the XSPEC X-ray spectral fitting software, and we thank the people who have created and maintain this software. This research has made use of the SIMBAD database, operated at CDS, Strasbourg, France and the NASA/IPAC extragalactic database (Helou et al. 1991) which is operated by the Jet Propulsion Laboratory, Caltech.

REFERENCES

Alloin D., Collin-Souffrin S., Joly M., Vigroux L., 1979, A&A, 78, 200
Anders E., Grevesse N., 1989, Geochimica et Cosmochimica Acta, 53, 197
Armus L., Heckman T.M., Weaver K.A., Lehnert M.D., 1995, ApJ, in press
Athanassoula E., 1992, MNRAS, 259, 345
Awaki H., Koyama K., 1993, Adv. Space Res., 13, 221
Baumgart C.W., Peterson C.J., 1986, PASP, 98, 56
Bland-Hawthorn J., Sokolowski J., Cecil G. 1991, ApJ, 375, 78
Bowyer S., Lieu R., Sidher S.D., Lampton M., Knude J., 1995, Nature, 375, 212
Brindle C., Hough J.H., Bailey J.A., Axon D.J., Ward M.J., Sparks W.B., McLean I.S., 1990, MNRAS, 244, 577
Brinkmann W. et al., 1994, A&A, 288, 433
Burstein D., Heiles C., 1978, ApJ, 225, 40
Calzetti D., Kinney A.L., Storchi-Bergmann T., 1994, ApJ, 429, 582
David L.P., Jones C., Forman W., 1992, ApJ, 388, 82
David L.P., Harnden F.R., Kearns K.E., Zombeck M.V., 1995, The ROSAT High Resolution Imager. GSFC, Greenbelt
Davies R.D., 1989, QJRAS, 30, 295
de Vaucouleurs G., 1975, in Sandage A., Sandage M., Kristian J., eds, Galaxies and the Universe, Univ. of Chicago Press, Chicago, p. 557
Díaz A.I., 1985, PhD thesis, University of Sussex
Elmegreem D.M., Sundin M., Elmegreen B., Sundelius B., 1991, A&A, 244, 52
Fabian A.C., Ward M.J., 1993, MNRAS, 263, 51P
Fabbiano G., 1988, ApJ, 330, 672
Fabbiano G., Feigelson E., Zamorani G., 1982, ApJ, 256, 397
Fabbiano G., Kim D.-W., Trinchieri G., 1992, ApJS, 80, 531
Forbes D.A., Ward M.J., DePoy D.L., Boisson C., Smith M.S., 1992, MNRAS, 254, 509
García-Vargas M.L., Díaz A.I., Terlevich R.J., Terlevich E., 1990, Astr. Space Sci., 171, 65
Griffiths R.E., Feigelson E., van Speybroeck L., 1979, Bull. Am. Ast. Soc., 11, 466
Halpern J., 1992, in Holt S.S., Neff S.G., Urry C.M., eds, Testing the AGN Paradigm. AIP Press, New York, p. 524
Harnden F.R., et al., 1979, ApJ, 234, L51
Harnett J.I., 1987, MNRAS, 227, 887
Hasinger G., Turner T.J., George I.M., Boese G., 1992, Legacy #2, The Journal of the High Energy Astrophysics Science Archive Research Center, NASA/GSFC
Heckman T.M., Armus L., Miley G.K., 1990, ApJS, 74, 833
Heckman T.M., Dahlem M., Lehnert M.D., Fabbiano G., Gilmore D., Waller W.H., 1995, ApJ, 448, 138
Helou G., Madore B.F., Schmitz M., Bicay M.D., Wu X., Bennett J., 1991, in Egret D., Albrecht M., eds, Databases and On-Line Data in Astronomy, Kluwer, Dordrecht, p. 89
Iwasawa K., Yaqoob T., Awaki H., Ogasaka Y., 1994, PASJ, 46, L167
Kawara K., Nishida M., Gregory B., 1987, ApJ, 321, L35
Kinney A.L., Bohlin R.C., Calzetti D., Panagia N., Wyse R.F.G., 1993, ApJS, 86, 5
Kruper J.S., Urry C.M., Canizares C.R., 1990, ApJS, 74, 347
Lampton M., Margon B., Bowyer S., 1976, ApJ, 208, 177
Lasker B.M., Sturch C.R., McLean B.J., Russell J.L., Jenkner H., Shara M.M., 1990, AJ, 99, 2019
Leene A., Cox P., 1987, A&A, 174, L1
Lequeux J., 1988, in Bailey M.E., Williams D.A., eds, Dust in the Universe, Cambridge Univ. Press, Cambridge, p. 449
Lindblad P.O., Jörsäter S., 1996, A&A, in preparation
MacLow M.-M., McCray R. 1988, ApJ, 324, 776
Maia M., Pastoriza M., Bica E., Dottori H., 1994, ApJS, 93, 425
Mathewson D.S., Rome J.M., 1963, Aust J Phys, 16, 360
Mathis J.S., 1990, ARA&A, 28, 37
Moorwood A.F.M., Oliva E., 1988, A&A, 203, 278
Morse J.A., 1994, PASP, 106, 675
Morse J.A., Wilson A.S., Elvis M., Weaver K.A., 1995, ApJ, 439, 121
Osmer P.S., Smith M.G., Weedman D.W., 1974, ApJ, 192, 279 (OSW74)
Pastoriza M.G., 1973, PhD thesis, Córdoba Instituto de Matemáticas, Astronomía y Física
Pfeffermann E. et al., 1987, Proc. SPIE, 733, 519
Press W.H., Flannery B.P., Teukolsky S.A., Vetterling W.T., 1989, Numerical Recipes in Pascal. Cambridge Univ. Press, Cambridge
Rangarajan F.V.N., White D.A., Ebeling H., Fabian A.C., 1995, MNRAS, submitted
Rosa M.R., Benvenuti P., 1995, A&A, in press
Sandage A., Bedke J., 1994, The Carnegie Atlas of Galaxies. CIOW Press, Washington D.C.
Sanders D.B., Soifer B.T., Elias J.H., Neugebauer G., Matthews K., 1988, ApJ, 328, L35
Sandqvist Aa., Jörsäter S., Lindblad P.O., 1995, A&A, 295, 585
Sérsic J.L., 1968, Atlas de Galaxias Australes. Córdoba Univ. Press, Córdoba
Sérsic J.L., Pastoriza M., 1965, PASP, 77, 287
Sérsic J.L., Calderón J.H., 1979, Ast. and Space Sci., 62, 211
Shafer R.A., Haberl F., Arnaud K.A., Tennant A.F., 1991, XSPEC Users Guide. ESA Publications, Noordwijk
Storchi-Bergmann T., Calzetti D., Kinney A.L., 1994, ApJ, 429, 572
Storchi-Bergmann T., Wilson, A.S., Baldwin, J.A., 1996, ApJ, in press (SWB96)
Tielens A.G.G.M., Allamandola L.J., 1987, in Hollenbach D.J., Thronson H.A., eds, Interstellar Processes, Reidel, Dordrecht, p. 397
Tovmassian H.M., 1966, Aust J Phys, 19, 883
Tovmassian H.M., 1968, The Observatory, 88, 227
Trümper J., 1983, Adv. Space Res., 4, 241
Turner T.J., George I.M., Mushotzky R.F., 1993, ApJ, 412, 72
Ulvestad J.S., Wilson A.S., 1984, ApJ, 285, 439
Véron M.P., Véron P., Zuiderwijk E.J., 1981, A&A, 98, 34
Wang Q., Helfand D.J., 1991, ApJ, 370, 541
Ward M.J., 1988, MNRAS, 231, 1P
Wilson A.S., Elvis M., Lawrence A., Bland-Hawthorn J., 1992, ApJ, 391, L75
Witt A.N., Thronson H.A., Capuano J.M., 1992, ApJ, 393, 611

SOFT X-RAY PROPERTIES OF THE BINARY MILLISECOND PULSAR J0437–4715

JULES P. HALPERN
Columbia Astrophysics Laboratory, Columbia University,
538 West 120th Street, New York, NY 10027
jules@carmen.phys.columbia.edu

CHRISTOPHER MARTIN
Downs Laboratory, California Institute of Technology, 220–47
Pasadena, CA 91125
cmartin@porgy.srl.caltech.edu

AND
HERMAN L. MARSHALL
Center for Space Research, Massachusetts Institute of Technology
37–667a, Cambridge, MA 02138
hermanm@space.mit.edu

Submitted to *The Astrophysical Journal*

Received _____; *accepted* _____

ABSTRACT

We obtained a light curve for the 5.75 ms pulsar J0437–4715 in the 65–120 Å range with 0.5 ms time resolution using the Deep Survey instrument on the *EUVE* satellite. The single-peaked profile has a pulsed fraction of 0.27 ± 0.05, similar to the *ROSAT* data in the overlapping energy band. A combined analysis of the *EUVE* and *ROSAT* data is consistent with a power-law spectrum of energy index $\alpha = 1.2-1.5$, intervening column density $N_{\rm H} = (5-8)\times 10^{19}$ cm^{-2}, and luminosity 5.0×10^{30} ergs s^{-1} in the 0.1–2.4 keV band. We also use a bright *EUVE/ROSAT* source only 4′.3 from the pulsar, the Seyfert galaxy RX J0437.4–4711 (= EUVE J0437–471 = 1ES 0435–472), to obtain an independent upper limit on the intervening absorption to the pulsar, $N_{\rm H} < 1.2 \times 10^{20}$ cm^{-2}.

Although a blackbody spectrum fails to fit the *ROSAT* data, two-component spectral fits to the combined *EUVE/ROSAT* data are used to limit the temperatures and surface areas of thermal emission that might make *partial* contributions to the flux. A hot polar cap of radius $50 - 600$ m and temperature $(1.0 - 3.3) \times 10^6$ K could be present. Alternatively, a larger region with $T = (4-12)\times 10^5$ K and area less than 200 km^2, might contribute most of the *EUVE* and soft X-ray flux, but only if a hotter component were present as well. Any of these temperatures would require some mechanism(s) of surface reheating to be operating in this old pulsar, the most plausible being the impact of accelerated electrons and positrons onto the polar caps. The kinematically corrected spin-down power of PSR J0437–4715 is only 4×10^{33} ergs s^{-1}, which is an order of magnitude less than that of the lowest-luminosity γ-ray pulsars Geminga and PSR B1055–52. The absence of high-energy γ-rays from PSR J0437–4715 might signify an inefficient or dead outer gap accelerator, which in turn accounts for the lack of a more luminous reheated surface such as those intermediate-age γ-ray pulsars may have.

Subject headings: pulsars: individual (PSR J0437–4715) – stars: neutron – X-rays: stars

1. INTRODUCTION

The 5.75 ms pulsar J0437–4715, discovered by Johnston et al. (1993), is the nearest millisecond pulsar at $d = 140$ pc, and is also in a 5.74 d binary orbit with a cool white dwarf companion of mass $\sim 0.2 M_\odot$ (Bailyn 1993; Bell, Bailes, & Bessell 1993; Danziger, Baade, & Della Valle 1993). Its radio emission is so bright that individual pulses are easily seen. It is also the only millisecond pulsar from from which pulsed X-rays have been detected (Becker & Trümper 1993), and one of two surrounded by a bow-shock nebula (Bell et al. 1993; 1995). Fundamental questions about PSR J0437–4715 and other millisecond pulsars are 1) whether or not its characteristic age, $P/2\dot{P}$, is consistent with the cooling age of its white dwarf companion, 2) whether its X-rays are magnetospheric in origin or thermally reheated surface emission, and 3) why it is not (yet) a detectable high-energy γ-ray source.

Accurate determinations of $\dot{P}$ and proper motion for PSR J0437–4715 have now been established (Bell et al. 1995; Bell 1995) that will have a major impact upon all of these mysteries. Its intrinsic $\dot{P}$ is 1.99×10^{-20}, only one third of the measured value of 5.72×10^{-20} after correcting for the "train whistle" effect (e.g., Camillo, Thorsett, & Kulkarni 1995), the kinematic contribution to the measured $\dot{P}$ from the pulsar's transverse velocity of 92 km s^{-1}. Interestingly, this effect also limits the distance to PSR J0437–4715 to an absolute maximum of 215 pc. Its characteristic age is 4.6×10^9 yr, 6 times longer than the original estimate (Johnston et al. 1993), and consistent with estimates of the age of its white dwarf companion. Furthermore, its spin-down power, $I\Omega\dot{\Omega}$, is only 4×10^{33} ergs s^{-1}, almost an order of magnitude smaller than first reported, and less than that of the lowest luminosity γ-ray pulsars by the same factor.

The nature of the soft X-ray emission from PSR J0437–4715 is still not clear. Becker & Trümper (1993) suggested that, in addition to the mostly power-law spectrum, a blackbody component of temperature $T \sim 1.7 \times 10^6$ K and emitting area 0.05 km^2 might be be present that they associated with a peak at 0.9 keV in the pulsed fraction as a function of energy. Such a component would, of course, demand the operation of some mechanism of surface reheating; in all calculations neutron stars cool below 10^5 K after 10^6 yr. Estimates of the magnetic dipole and viewing geometry, albeit uncertain ones, were made by Manchester & Johnston (1995) using the rotating vector model of the radio polarization, which can aid in the interpretation of the X-ray pulse profile.

In this paper, we report the results of a long *EUVE* observation of PSR J0437–4715, together with a reanalysis of the *ROSAT* PSPC observation of the same source. A previous, shorter *EUVE* observation of PSR J0437–4715 was reported by Edelstein, Foster, & Bowyer (1995), but those data were not taken in the high time resolution mode which is necessary to see the pulsations. Furthermore, combined analysis of the *EUVE* and *ROSAT* pulse profiles and spectra enable us to reassess the question of thermal vs. nonthermal X-ray emission, and to place formal limits on the properties of any thermal components that may be present.

2. *EUVE* OBSERVATIONS AND TIMING ANALYSIS

The pulsar J0437–4715 was observed by *EUVE* during a 20 day period between 1994 October 23 and November 12, during which a valid exposure time of 495,897 s was obtained in the Deep Survey (DS) instrument. Events occurring when the line of sight to the source passed less than 400 km above the Earth's limb were rejected. A total of 4370 counts above background were collected from the pulsar through the Lexan filter, as determined in a 73″ radius extraction aperture. After accounting for deadtime and "Primbsching," the effective exposure time is reduced to 449,034 s. The resulting corrected count rate of 0.00973 s^{-1} was used in all calculations that require an absolute flux. To maximize the signal-to-noise ratio in the pulsed light curve, we also extracted counts within a smaller aperture of the DS, a carefully placed circle of radius 43″ which contains 95% of the source counts in the asymmetric source profile. The resulting light curve contains an estimated 4163 source counts, and only 937 background events.

Data were taken simultaneously by the three spectrometers pointed at the source, but no significant detection of the pulsar was made in these. The spectrometer data will not be discussed further here.

An updated pulsar and binary orbit ephemeris, including an accurate position, were kindly supplied by J. F. Bell. Millisecond pulsars are extremely stable clocks, and the radio ephemeris is accurate to 5 μs for the entire three-year period since the discovery of the pulsar. We first transformed the time of arrival of each photon to Barycentric Dynamical Time (TDB) using a procedure based on the Princeton TEMPO code, supplemented with the additional corrections for the changing orbital position of the *EUVE* satellite. The photon times were then corrected for the orbital Doppler delay within the 5.74 d binary system. The resulting pulse profile is shown in Figure 1. Background has been subtracted, and two cycles are graphed to guide the eye. There is one broad pulse per cycle, although it is narrower than a sinusoid. The pulsed fraction, defined conventionally as the fraction of the total counts lying above the minimum of the light curve, is 0.27 ± 0.05. The peak-to-trough ratio is approximately 1.8.

It is important to understand the possible sources of systematic error in the pulse profile in terms of the various effects that limit the accuracy of the final timing solution. A measurement of the pulse shape of this 5.75 ms pulsar is possible only because the observation was made in "WSZ" mode, which tags each photon with the full 0.5 ms time resolution of the the spacecraft clock. Although the spacecraft clock drifts at an average rate of $\sim 1 \times 10^{-8}$, the times in the data stream are kept to within ± 0.3 ms of UTC by the following procedure. Each time the clock drifts to +0.3 ms, a jump of –0.6 ms is applied to the data. This correction is applied on average 3.2 times per day. During the span of our observation, 61 such corrections were applied. By interpolating between these known discontinuities, we reduced this particular source of error to ~ 0.1 ms, resulting in a slightly sharper pulse profile. Another requirement for limiting systematic errors to 0.1 ms is knowledge of the satellite ephemeris to an accuracy of 30 km along its orbit. This condition has not been verified to our knowledge, but the design specification of 10 km is well within our requirements. Since the time resolution is still no better than 0.5 ms, fine details in the pulse profile may not be significant. In particular, the 20 bin light curve in Figure 1 oversamples the true time resolution by a factor of 2.

Even though we believe that the *relative* stability of the spacecraft clock was maintained to better than 0.5 ms over the 20 day span of the observation, the details of the pulse profile could also be affected by errors in *absolute* timing, if there are any. We do not believe that there are any such gross effects. For example, the *EUVE* data can itself be used to time the periastron passage of the pulsar, and it agrees with the radio ephemeris to within ± 15 s. Any errors in absolute time that are smaller than this would have a negligible effect on our results.

In deriving the pulse profile in Figure 1, it is important that we deliberately *did not* search over a range of pulsar and binary parameters, since the radio ephemeris is extremely accurate for our purposes. Unlike the radio, the X-ray pulse does not have a strong, narrow feature that can be used to optimize the ephemeris. Such a search would simply introduce large, spurious features into the pulse profile. In summary, we believe that the light curve in Figure 1 is grossly accurate in terms of pulsed fraction and non-sinusoidal shape, but that the individual bin-to-bin variations are not reliable. In particular, it is not clear if the top of the light curve is flat, cusped, or round.

3. *ROSAT* OBSERVATIONS AND TIMING ANALYSIS

The *ROSAT* PSPC observation of PSR J0437–4715 was originally reported by Becker & Trümper (1993). We have reanalyzed this observation in order to make joint spectral fits of the *ROSAT* and *EUVE* data for this presumably steady source, and to compare the pulse profile with the one from *EUVE*. A total exposure of 6142 s was obtained during three satellite orbits on 1992 September 20 and 21. Extraction of the source counts is relatively straightforward, except that at energies below 0.15 keV the electronic "ghost imaging" can smear the photon positions by as much as $2'.5$ from the centroid position. This particular observation is problematic because of the presence of a brighter soft X-ray source $4'.3$ from the pulsar, the former being the target of the observation in which the pulsar appeared serendipitously. As a compromise which extracted virtually all of the counts from the pulsar with negligible contamination from the neighboring source, we used a $1'.75$ extraction radius, and obtained a background measurement from a source-free circle with 4 times larger area, but located at a similar off-axis angle. The derived background is less than 5% of the source counts at all energies. The off-axis vignetting correction at this position for all energies

of interest is less than 2%, and was neglected. A net total of 1254 photons were detected in the 0.08–2.0 keV band, for an average count rate of 0.20 s^{-1}. There is no detection above 2.0 keV. A 3% correction for deadtime was applied in all calculations that require absolute fluxes.

Although the time resolution of the PSPC data is $\sim 130\mu s$, timing analysis of a millisecond pulsar is more problematic with *ROSAT* than with *EUVE*. The drift rate of the *ROSAT* spacecraft clock is $\sim 8 \times 10^{-8}$, an order of magnitude larger that that of *EUVE*, yet it was calibrated only once per week on average, as opposed to three times per day for *EUVE*. Inspection of the calibration data (e.g., Predehl 1994) reveals that nonlinearities in the drift rate cause residual errors of up to 2 ms per week that cannot be removed by fitting low-order functions to the calibration points. Furthermore, it is not clear that the day-to-day predictability of the spacecraft clock is much better than 1 ms.

Of the three spacecraft orbits that constitute the *ROSAT* observation of PSR J0437–4715, two are adjacent, but one came exactly 1 day (15 orbits) earlier. After performing the barycentric correction using the spacecraft clock calibrations contained in the PROS version 2.3.1 software, we folded the pulsar data separately for the three spacecraft orbits. Not surprisingly, the two adjacent orbits show pulse profiles which agree in phase, while the orbit separated by one day has a statistically significant phase offset of approximately 0.5 ms. Since the magnitude of this offset is typical of what is expected for clock drift, we interpreted it as such, and shifted the first orbit's data by 0.5 ms before coadding to make the final pulse profile shown in Figure 2. Subsequent details of our analysis are not significantly affected by this somewhat arbitrary procedure.

Our pulse profile is similar to that found by Becker & Trümper (1993). They found that the pulsed fraction is a strong function of energy, with an average of 0.30 ± 0.03 over the full *ROSAT* energy range, and a peak of 0.53 ± 0.06 in the 0.6–1.1 keV band. We find a slightly weaker dependence. The average pulsed fraction is 0.32 ± 0.05, and the sub-intervals illustrated in Figure 2 have pulsed fractions of 0.35 ± 0.04, 0.47 ± 0.09, and 0.19 ± 0.10, respectively, in the 0.08–0.53, 0.53–1.10, and 1.10–2.00 keV bands. The *EUVE* pulsed fraction of 0.27 ± 0.05 is not significantly different from the value of 0.30 ± 0.10 that can be measured from the smaller number of photons in the overlapping *ROSAT* band (0.08–0.20 keV). The error bars are dominated by the uncertainty in establishing the minimum in the light curve, and are estimated by eye. In summary, we have at most weak evidence for an increase in pulsed fraction from 0.27 at 0.1 keV to 0.47 at 1 keV. Above 1 keV, the statistics are too poor to determine a pulsed fraction.

The slight differences between our results can largely be explained by methodology. Becker & Trümper (1993) fitted sinusoids, while we used the more standard definition (counts above minimum) which is less dependent upon pulse shape. In any case, the evidence for an energy-dependent pulsed fraction is not as strong as the peak in Figure 2 of Becker & Trümper (1993) might lead one to believe, because the adjacent points in that figure are not independent, and because the peak is narrower than the resolution of the detector. It is also possible that their results differ from ours because they varied the longitude of periastron in their pulsar search to optimize some measure of the "best" fit. As we have argued above, such a procedure is not warranted, and could introduce spurious features into the pulse profile. If the pulse *shape* differs with energy, this would be a reason to reassess both of our methods of determining the pulsed fraction, and the meaning of the results. But as pointed out by Becker & Trümper (1993), there is no strong evidence for energy dependence in the pulse shape or phase. In summary we believe that there could be a weak dependence of pulsed fraction on energy. Our enthusiasm for fitting more than one component to the spectrum is somewhat dampened, but not completely drowned (see §4.2).

Since we are not yet confident about the *absolute* timing of the *ROSAT* data at the 1 ms level (or the *EUVE* data, for that matter), we do not attempt here to align the pulses in absolute phase with each other, or with the radio pulse.

4. COMBINED SPECTRAL ANALYSIS

There are likely pitfalls in fitting the *EUVE* and *ROSAT* data jointly because the nature of the error bars are completely different. The DS flux constitutes a single data point with very high statistical accuracy, but potentially disastrous systematics. The *ROSAT* error bars, on the other hand, are dominated by counting statistics. Therefore, we have chosen to apply a method in which

the *ROSAT* spectrum is first fitted over a generous grid of parameters, and then each of these trial spectra are folded thorough the DS effective are curve in order to find those models which are consistent with both instruments' data. In this way, the qualitatively different contribution of each to the errors can be seen. Only energies between 0.11 keV and 2.00 keV are included in the *ROSAT* spectral fits, corresponding to channels 3–30 in the standard 34 channel binning scheme. The 1993 January 12 response matrix was used. In all the Figures, channels 2–30 are displayed, but the channel 2 is not used in the fit. For the DS, the effective area curve used is that displayed in the Second *EUVE* Source Catalog (Bowyer et al. 1995).

4.1. *Single-Component Models*

As found by Becker & Trümper (1993), a single blackbody model gives an unacceptable fit to the *ROSAT* data, with $\chi^2 = 80$ for 25 degrees of freedom, $T = 1.5 \times 10^6$ K, and $N_{\rm H} = 0$. A simple power law gives an adequate fit, with $\chi^2 = 19.6$. Both fits are shown in Figure 3. The 90% confidence contour for the parameters of the power-law fit is shown in Figure 4. The best fitted column density of 9×10^{19} cm^{-2} is consistent with the dispersion measure of 2.65 cm^{-3} pc and a hydrogen ionization fraction of 0.1. The energy spectral index $\alpha = 1.45 \pm 0.25$ is consistent with the value of 1.6 ± 0.2 found by Becker & Trümper (1993), but our intrinsic luminosity of 5.0×10^{30} ergs s^{-1} in the 0.1–2.4 keV band ($d = 140$ pc) is about 17% less than theirs.

The fact that the target of this *ROSAT* observation was actually a soft X-ray-selected Seyfert galaxy from the *ROSAT* All-Sky Survey (RX J0437.4–4711), affords a serendipitous measurement of the total Galactic X-ray absorption on a line of sight only 4'.3 from PSR J0437–4715. A power law fitted the spectrum of this bright Seyfert very well, with $\chi^2_\nu = 0.905$, $f_{\rm x} = 1.47 \times 10^{-11}$ ergs cm^{-2} s^{-1}, $\alpha = 1.56 \pm 0.09$, and $N_{\rm H} = (1.01 \pm 0.16) \times 10^{20}$ cm^{-2}. We consider this value of $N_{\rm H}$ to be a reliable upper limit on the X-ray absorption to the pulsar, subject only to the caveat that $N_{\rm H}$ might be larger if there is really an unmodelled upturn in the soft X-ray spectrum of the Seyfert that makes it steeper than the fitted power law. For this source, we do not attempt a joint fit to the *EUVE* and *ROSAT* data taken 2 years apart because Seyfert galaxies are notoriously variable, especially those with very soft spectra. Such a comparison would likely be meaningless. Instead, a detailed analysis of the long *EUVE* light curve of this Seyfert galaxy is reserved for a later paper. We also note that RX J0437.4–4711 should be identified with EUVE J0437–471 as listed in the Second *EUVE* Source Catalog (Bowyer et al. 1995), and with the *Einstein* Slew Survey source 1ES 0435–472 (Elvis et al. 1992), whose position is consistent with that of the *ROSAT* source.

In order to test whether or not the *EUVE* flux of PSR J0437–4715 is consistent with the power-law fit to the *ROSAT* spectrum, we folded each of the trial *ROSAT* spectra corresponding to the fixed grid of Figure 4 through the effective area curve of the DS. The normalization constant for each trial was individually calculated from the total *ROSAT* counts. In this way, a grid of predicted DS counts was derived for comparison with the observed number. The range of spectral parameters acceptable to the DS is approximated by assigning a ±15% uncertainty to the predicted DS count rate to account for any relative errors in normalization between the effective areas of the two instruments. The resulting band of spectral parameters allowed by the DS overlaps the *ROSAT* confidence contour in Figure 4, implying that a single power law fits both instruments.

The principal contribution of the *EUVE* point is to restrict $N_{\rm H}$ to the lower end of the *ROSAT* range, namely $(5 - 8) \times 10^{19}$ cm^{-2}. This is consistent with what we know about the total column density in this direction from the adjacent Seyfert galaxy, which has $N_{\rm H} = (1.01 \pm 0.16) \times 10^{20}$ cm^{-2}, and with the dispersion measure that indicates an ionized column of $N_{\rm e} \sim 8 \times 10^{18}$ cm^{-2} toward the pulsar. At a Galactic latitude of −42°, the 140 pc line of sight to the pulsar passes through a neutral gas column about half that to infinity. Thus, the measured range of $(5 - 8) \times 10^{19}$ cm^{-2} is within expected limits.

Although the DS Lexan band is sensitive in the range 65–200 Å, photons are detected from PSR J0437–4715 only at the short wavelength end because of the steep increase in interstellar absorption as a function of wavelength. Figure 5 shows the effective distribution of detected counts from PSR J0437–4715 in the DS corresponding to the range of power-law models that fitted, with their correct normalizations, both the *ROSAT* and DS fluxes. Since nearly all the detected flux is at wavelengths shortward of 120 Å, we refer to this band conventionally as soft X-rays.

Our result contradicts the claim of Edelstein *et al.* (1995) that their earlier *EUVE* observation is inconsistent with a power-law fit to the *ROSAT* data unless the column density is as high as 2.5×10^{20} cm^{-2}, an unacceptably large value. We can only speculate that their conclusion was based on the use of the slightly more luminous and steeper power law reported by Becker & Trümper (1993), without regard to the *range* of individual normalizations that would be associated with a grid of acceptable fits. Our own power-law folds though both instruments are consistent with $N_{\rm H} = (5-8)\times10^{19}$ cm^{-2}.

Given the acceptable fit of a single power law with reasonable column density to both the *EUVE* and *ROSAT* data, and the lack of evidence for a blackbody component, one would be tempted to call a halt to the spectral fitting at this point. In fact, the $\chi^2_{\rm min}$ of the power-law model is almost *too* small. The probability of χ^2 exceeding the observed value of 19.6 is 77%. Therefore, the statistical quality of the data may not be good enough to support tests for deviations from a power law. Nevertheless, there are weak observational reasons, and strong theoretical reasons, to examine what contribution a blackbody component *might* make to the soft X-ray flux without violating observed limits. The observational reasons are the possible variation in pulsed fraction as a function of energy, and the fact that the peaks are not so strong and sharp as to rule out a contribution of a hot surface to either the pulsed or the unpulsed flux. The theoretical reason has do with estimates of polar cap heating from the impact of particles accelerated in the pulsar magnetosphere that predict thermal luminosities which are not insignificant compared to the observed X-ray luminosity of PSR J0437–4715. That some younger pulsars seem to display such components is also a motivation to examine such a scenario. Accordingly, we analyze two-component models in the following sections, one involving a power law plus blackbody, and the other a pair of blackbodies.

4.2. *Power Law plus Blackbody Model*

Becker & Trümper (1993) argued that a spectral decomposition in which a blackbody made a significant contribution to the flux between 0.6 and 1 keV was acceptable, and was motivated by the increase in pulsed fraction at these energies. Although we think that the evidence for an energy-dependent pulsed fraction is not so definitive, we nevertheless explore the possible range of power law plus blackbody fits to the spectrum. The model spectrum takes the form

$$F(E) = C\left(\frac{E^3}{e^{E/kT}-1} + f\,E^{-\alpha}\right)e^{-\sigma(E)N_{\rm H}}\ \ {\rm keV\,cm^{-2}\,s^{-1}\,keV^{-1}}. \qquad (1)$$

The method that we use in exploring the parameter space of this model is the same as that described in Halpern & Ruderman (1993) for the Geminga pulsar. Briefly, a full four-dimensional χ^2 grid is searched for acceptable values of the temperature T, energy spectral index α, column density $N_{\rm H}$, and power-law fraction f. For each trial spectrum, the overall normalization constant C is that which matches the total counts. Confidence limits can then be found by projecting the χ^2 grid onto any lower dimensional surface of interest.

The best such model is shown in Figure 6, and the 90% confidence contour for the blackbody component in the $(T, N_{\rm H})$ plane is shown in Figure 7. The decrease in $\chi^2_{\rm min}$ from 19.6 (in the power-law fit) to 12.8 justifies the addition of two parameters at the 99% level, according to the F test. However, this $\chi^2_{\rm min}$ is probably *too* small, as discussed above. The probability of χ^2 exceeding 12.8 is 95.6%. A column density less than 10^{19} cm^{-2} is formally possible in this model because the blackbody has an intrinsic downturn at low energy. Such a low value is conceivable if most of the interstellar medium in the line of sight is in the hot phase, a possibility which is not contradicted by any measurement that we are aware of.

If we adopt the dispersion-measure distance of 140 pc, then each trial fit can be translated to a surface area for the blackbody component. Because the fitted temperatures are relatively large, $T = (1.0-3.3)\times10^6$ K, the corresponding surface areas are quite small. The radius of the inferred hot spot ranges from 50–600 m, as indicated by the dashed contours in Figure 7, and its bolometric luminosity is $\sim 8.4\times10^{29}$ ergs s^{-1}. In comparison, the standard radius of the open field-line polar cap, $r_{\rm p} = (R\Omega/c)^{1/2}R$, is 1.9 km. Note that these area estimates are uncertain by a factor of a few because of the time-averaged projection effects that depend on the unknown viewing geometry of the assumed small, hot region. We also neglect the possible deviations of

realistic model atmospheres from a blackbody, which tend to lower the temperatures that can fit a given observed spectrum (Romani 1987; Miller 1992). The results of this model are similar to those of Becker & Trümper (1993), who found a temperature of $\sim 1.7 \times 10^6$ K and an emitting area of 0.05 km^2 ($r \sim 125$ m). But Figure 7 shows the full range of parameters allowed by this fit. In view of the weak need for a thermal component to begin with, the areas could be interpreted as upper limits rather than estimates.

Finally, we superpose a contour that corresponds to agreement with the observed *EUVE* DS flux. As before, the main contribution of the DS measurement is to restrict the column density to less than 8×10^{19} cm^{-2}. It is important to realize that, in this model, it is still the power law that makes the dominant contribution to the *EUVE* detection. Figure 6 shows that the thermal component contributes less than 10% of the flux below 0.2 keV. At 0.7 keV, however, the thermal contribution is about 40% of the total, which could be consistent with the slight increase in pulsed fraction at that energy (47% as opposed to $\sim$ 32% on average). This scenario would require the thermal component to be more highly pulsed than the power law, and nevertheless have the same phase. In §5.2, we consider the related hypothesis that some of the steady, power-law X-ray flux might originate in the bow shock.

4.3. *Double Blackbody Model*

It is possible for both the *EUVE* flux and "soft" *ROSAT* band to be dominated by blackbody emission, but only if the "hard" *ROSAT* flux is a separate blackbody component, and not a power law. Following the same method as in the previous section, we searched a four-dimensional parameter space of two temperatures, T_1 and T_2, column density $N_{\rm H}$, and fraction f which is closely related to the ratio of surface areas A_2/A_1 of the two blackbody components. The form of the model spectrum is

$$F(E) = C\,E^3 \left(\frac{1}{e^{E/kT_1} - 1} + \frac{f}{e^{E/kT_2} - 1} \right) e^{-\sigma(E) N_{\rm H}} \ \ {\rm keV\,cm^{-2}\,s^{-1}\,keV^{-1}}. \qquad (2)$$

Figure 8 is an example of the best such fit, and Figure 9 shows the allowed spectral parameters for the *softer* blackbody ($T_1, N_{\rm H}$). The decrease in $\chi^2_{\rm min}$ from 19.6 in the power-law fit to 14.5 justifies the addition of two parameters at the 97% level, according to the F test. As before, contours of surface area A_1 for the softer blackbody are superposed as dashed lines in Figure 9. The ratio of areas A_2/A_1 (not shown) ranges from $10^{-4} - 10^{-2}$ in all cases.

The effect of the *EUVE* point is, as before, to restrict the column density to less than 8×10^{19} cm^{-2}. The overlap between the *EUVE* and *ROSAT* contours restricts the soft blackbody parameters to the range $4 \times 10^5 < T_1 < 12 \times 10^5$ K, and $2 < A_1 < 200$ km^2. Thus, the upper limit on the emitting area is less than 20% of the typical area of a neutron star, and may be comparable to that of the open field-line polar cap, ~ 11 km^2 for this rotation period.

In this model the softer blackbody component dominates the *EUVE* DS flux and *ROSAT* PSPC carbon band with a bolometric luminosity of $L_1 \sim 1.8 \times 10^{30}$ ergs s^{-1}, while the harder component with $L_2 \sim 1.5 \times 10^{30}$ ergs s^{-1} dominates the PSPC spectrum above 0.5 keV. This is an important distinction from the previous model, in which the power-law component makes the major contribution across the entire observed band. While the double blackbody model dispenses with the power-law component entirely, it leaves us with the question of why two thermal components that differ in area by several orders of magnitude should produce pulse profiles that are so similar. However, as long as both areas are concentric and much smaller than the neutron star, the resulting pulse shapes are expected to be the same. Alternatively, nature might be more realistic by employing a continuous range of temperatures in a way that produces a roughly energy-independent pulse shape. Finally, we remind the reader (and ourselves) that we embarked upon an investigation of these two-component models only to develop upper limits on thermal components. Perhaps they don't exist at all.

5. INTERPRETATION

5.1. *Pulse Profile and Dipole Geometry*

Possible interpretations of the X-ray pulse profile include hot spots at the magnetic polar caps, and beaming of nonthermal radiation along the open magnetic field lines. Quite specific information about the magnetic geometry and viewing direction of pulsars can be derived from the rotating vector model of the radio polarization, which often represents the sweep of position angle with phase very well. In the case of PSR J0437–4715, there is significant radio emission over at least 80% of the pulse period, but the complex details of the position angle variations are not fitted well by the simple model (Manchester & Johnston 1995). Deviations are not unexpected from millisecond pulsars, since the emission region is likely to be close enough to the surface for higher order multipoles of the magnetic field to have a significant effect on the polarization. Although the pulse profile is itself complex, Manchester & Johnston concluded that the strong "core" component indicates that the magnetic axis crosses close to our line of sight. Despite possible complicating details, they conclude that the overall shape of the position angle variation favors magnetic inclination angle $\alpha = 145°$, and viewing angle $\zeta = 140°$, both measured from the rotation axis. In this geometry, and for a dipole centered on the star, the opposite magnetic pole remains more than 15° below the limb at all times, which is consistent with the absence of an interpulse in the radio, and in the X-ray if the latter is at least moderately beamed.

This geometry does not clearly distinguish between thermal and nonthermal models for the X-ray pulse for two reasons. First, thermal emission from the opposite polar cap may still be visible because of strong light bending at the surface of the neutron star. Indeed, such an effect may be responsible for some of the substantial X-ray emission seen at pulse minimum. Detailed modelling of the light bending effect in this specific geometry for various assumed values of M/R would be necessary to determine whether the observed pulse profile is consistent with thermal emission from both poles. Second, the simple centered dipole may not be a correct description of the *surface* magnetic field geometry, even to a first approximation. Indeed, there are theoretical reasons to think that this is the case for millisecond pulsars (Chen & Ruderman 1993), and observations of thermal X-ray components in ordinary pulsars always show only one pulse per rotation period (e.g., Halpern & Ruderman 1993). As mentioned earlier, the coincidence of the X-ray phase at all energies is problematic for models in which both thermal and nonthermal processes contribute. Time of flight delays and differential relativistic aberration between the pulsar's surface and magnetosphere are substantial. Ultimately, the absolute time of arrival of the X-ray pulse with respect to the radio will reveal important information about the relative heights of the radio and X-ray emitting regions, but this analysis is not yet reliable at the ms level. For these reasons, we must rely on the X-ray spectrum for additional clues about the sources of emission.

5.2. Sources of Nonthermal Emission

If most of the soft X-ray emission from PSR J0437–4715 is to be described as a nonthermal power law, then it must flatten in the far ultraviolet so as not to exceed the observed brightness of the $B = 22$ optical companion (Bell et al. 1993; Danziger et al. 1993). The X-ray power law of slope 1.45 would extrapolate to $B = 16.7$. A power law connecting the actual blue flux to the observed X-ray flux at 200 eV would have a spectral index of 0.30. The real ultraviolet spectrum must therefore be flatter on average than 0.3. The X-ray and assumed far UV spectrum could be synchrotron radiation in the $< 3.4 \times 10^8$ G magnetic field near the surface of the neutron star, as the cyclotron frequency eB/mc falls in the visible band. Electrons with Lorentz factor $\gamma \gtrsim 10$ would produce the soft X-rays that we see. Alternatively, synchrotron emission from the outer magnetosphere, within the light cylinder of radius $r_{lc} = 2.7 \times 10^7$ cm, could involve electrons of $\gamma \gtrsim 2000$ and $B \sim 10^4$ G. Our default interpretation is that most of the X-ray flux from PSR J0437–4715 is magnetospheric in origin, similar to that of ordinary, young pulsars, with the rather low pulsed fraction perhaps resulting from a broader beaming pattern related to the large opening angle of the open field-line region expected for millisecond pulsars, and observed in the radio.

The observed flux and its plausible extrapolations to low and high energies account for a negligible fraction of the spin-down power of the pulsar, $I\Omega\dot{\Omega} = 4 \times 10^{33}$ ergs s^{-1}. The *SIGMA* telescope aboard the *GRANAT* spacecraft derived an upper limit of 7×10^{32} ergs s^{-1} in the 40–200 keV range (Barret et al. 1994), which is not very restrictive. More significantly, an upper limit of 1.7×10^{32} ergs s^{-1} above 100 MeV can be deduced from the first 2 1/2 years of EGRET data (Fierro et al. 1995; Thompson et al. 1995), which means that PSR J0437–4715 is a significantly

less efficient high-energy γ-ray emitter than the middle-aged pulsars Geminga and PSR B1055–52. Leaving aside the possible importance of beaming geometry, it could be the case that, as speculated by Ruderman et al. (1993), pulsars channel an increasing fraction of their spin-down power into γ-ray luminosity until both approach $\sim 3 \times 10^{34}$ ergs s^{-1}, at which point the outer gap accelerator turns off. Since PSR J0437–4715 is an order of magnitude weaker in its spin-down power than Geminga and PSR B1055–52, both of which have $I\Omega\dot{\Omega} = 3 \times 10^{34}$ ergs s^{-1}, it may lie well to the wrong side of the outer-gap death line.

As is probably the case for most pulsars, the majority of the spin-down power is carried out in a wind of relativistic particles that ultimately deposits its energy in the interstellar medium. In the case of PSR J0437–4715, there is a direct quantitative measure of this process in the form of a bow-shock nebula (Bell et al. 1993; 1995) that points in the direction of the proper motion. We can use the usual argument that equates the ram pressure of the interstellar medium to the pulsar wind pressure at the apex of the bow shock to solve for the density of the ambient medium,

$$\rho_0 = \frac{I\Omega\dot{\Omega}}{4\pi\, r_{\rm w}^2\, v_{\rm p}^2\, c}. \tag{3}$$

Here $r_{\rm w}$ is the distance from the pulsar to the apex of the bow shock, and $v_{\rm p}$ is the velocity of the pulsar. Since lower limits to $r_{\rm w}$ and $v_{\rm p}$ are accurately known (projected values of 1.9×10^{16} cm and 92 km s^{-1}, respectively), an upper limit of 3.6×10^{-25} g cm^{-3} can be derived for ρ_0, corresponding to $n_{\rm H} \leq 0.15$ cm^{-3}. Since we do not imagine $n_{\rm H}$ to be much less than this upper limit, a large fraction of $I\Omega\dot{\Omega}$ must be dissipated by the shock.

The pulsar's velocity is too low to account for any of the unpulsed X-ray flux as post-shock thermal emission. But since the observed X-ray luminosity of PSR J0437–4715 is only $\sim 10^{-3} I\Omega\dot{\Omega}$, it is possible that some of the unpulsed X-ray flux might be synchrotron emission from relativistic electrons and positrons of $\gamma \sim 10^7$, radiating in the magnetic field of $\sim 2 \times 10^{-5}$ G that would be pulled out in equipartition with the wind from the light cylinder to the location of the shock. Particles can be accelerated to this energy because the maximum potential drop generated by the pulsar, $\Delta V_{\rm max} \sim (\Omega^2 B R^3)/(2c^2)$, is $\sim 6.7 \times 10^{13}$ V, corresponding to $\gamma \simeq 10^8$. This mechanism has been invoked to explain the weak X-ray flux from the only other millisecond pulsar to be detected in X-rays, PSR B1957+20 (Kulkarni et al. 1992). But since the X-ray luminosity in that case, $\sim 8 \times 10^{30}\, (d/1\,{\rm kpc})^2$ ergs s^{-1}, is only $\sim 10^{-4}$ of the spin-down power, PSR B1957+20 is perhaps not a precedent for expecting shock emission to contribute to the X-ray spectrum of PSR J0437–4715. Furthermore, the X-rays from PSR B1957+20 appeared not to be spatially extended in a *ROSAT* HRI image (Fruchter et al. 1992). Nevertheless, extended emission from the nebula at the analogous level of $\sim 4 \times 10^{29}$ ergs s^{-1} is certainly worth looking for in a long *ROSAT* HRI exposure of PSR J0437–4715.

5.3. Thermal Emission and Surface Reheating

The two-component models investigated here favor blackbody emission at temperatures of either $(4 - 12) \times 10^5$ K, or $(1.0 - 3.3) \times 10^6$ K, and from areas that are much smaller than the full surface of the neutron star. If these are taken as detections rather than upper limits, it would mean that thermal reheating is taking place, as neutron stars in all standard calculations cool below 10^5 K after 10^6 yr. A number of proposed thermal reheating mechanisms were evaluated by Edelstein et al. (1995) to account for the putative thermal component. These included 1) dissipation of internal heat generated by unpinning of vortex lines, 2) accretion from the interstellar medium, 3) accretion from the white-dwarf companion, 4) and nucleon decay catalyzed by magnetic monopoles. They found the first three of these to be inadequate, and we will not consider them further here, except to remark that their statement that "standard frictional heating models are virtually ruled out" is misleading. The heating rates produced by those models may be perfectly correct, but *additional* sources of heat may be necessary to account for the observed luminosity of PSR J0437–4715. A particular model can be proven defective only if predicts more heat than is observed, not if it predicts less.

The observation that the thermally emitting region must be comparable to or smaller than the open field-line polar cap, of radius $r_p = 1.9$ km, motivates us to consider another type of surface reheating, the bombardment of the polar cap region by energetic particles produced in the accelerators that are responsible for radio and high-energy emission. Direct evidence for such a process is seen in the X-ray emission from Geminga (Halpern & Ruderman 1993) and other intermediate-age pulsars (Finley 1994; Ögelman 1994), and especially from PSR B1929+10 (Yancopoulos, Hamilton, & Helfand 1994), a 3×10^6 yr old pulsar in which the 3×10^6 K blackbody emission comes from an area less than 50 m in radius. The same mechanism may also explain the weak X-ray flux from the 1.7×10^7 yr old pulsar PSR B0950+08 (Manning & Willmore 1994).

The maximum efficiency of heating by magnetospheric processes can be estimated following Halpern & Ruderman (1993). We multiply the Goldreich-Julian current density by the area of the polar caps to find an upper limit on the impacting particle flux,

$$\dot{N} < 2 \left(\frac{\Omega B}{2\pi e}\right) \left(\frac{\pi}{2}\frac{R\Omega}{c}\right) R^2 = 1.4 \times 10^{31} \text{ s}^{-1}. \quad (4)$$

The residual energy with which those particles impact the polar cap after radiating most of their energy via curvature radiation is,

$$E = \left[\frac{2e^2\,\Omega}{mc^3} \ln\left(\frac{r_{\rm in}}{R}\right)\right]^{-1/3} mc^2 \sim 2.3 \text{ ergs}, \quad (5)$$

Here, $r_{\rm in}$ is the inner radius of the accelerator region, which we take to be $\sim 10^7$ cm in this case. The maximum power brought down to the polar cap is then $L_p = \dot{N}E \leq 3.2 \times 10^{31}$ ergs s^{-1}.

This maximum heating rate is undoubtedly not operating because, if it were, the same accelerated particles would be radiating nearly the full spin-down power of PSR J0437–4715 in high-energy γ-rays. Rather, we suppose that the upper limit $L_\gamma < 1.7 \times 10^{32} = 0.04\, I\Omega\dot{\Omega}$ implies that either the size or the efficiency of the accelerator is less than 0.04 times the maximum value. Scaling the surface heating rate accordingly yields $L_p < 1.3 \times 10^{30}$ ergs s^{-1}. This is a comfortable value, for it can accommodate an interpretation of part of the observed X-ray luminosity as thermal without violating any of the upper limits. We conclude that even though the evidence for a thermal component is weak, a fraction of the observed X-ray luminosity could be understood as arising from the polar caps heated by particles accelerated in the magnetosphere without violating observational limits on γ-ray emission.

6. SUMMARY

The main purpose of this investigation was to examine the origin of the soft X-ray flux in the 5.75 ms pulsar J0437–4715. Plausible alternatives include magnetospheric synchrotron emission, surface thermal emission, and, for the unpulsed flux only, synchrotron emission at the pulsar wind's bow shock. Unfortunately, it is still not possible to rule out significant contributions from any of these mechanisms, as the light curve and spectrum do not strongly discriminate among them. The light curve in the *EUVE* DS (65–120 Å) consists of a single broad pulse containing $\sim 27\%$ of the flux, similar to that of the *ROSAT* data in the overlapping energy band. A combined analysis of the *EUVE* and *ROSAT* data is consistent with a power-law spectrum of intrinsic luminosity 5×10^{30} ergs s^{-1} in the 0.1–2.4 keV band, and $\alpha = 1.2 - 1.5$. The effect of the *EUVE* flux is to limit the column density $N_{\rm H}$ to the range $(5-8) \times 10^{19}$ cm^{-2}. For comparison, a nearby soft X-ray Seyfert galaxy determines the total Galactic column in this direction, $N_{\rm H} = 1 \times 10^{20}$ cm^{-2}.

When we apply two-component spectral fits to the combined *EUVE/ROSAT* data, we find that a small, hot polar cap of radius 50–600 m and temperature $(1.0-3.3) \times 10^6$ K could also be present. The principal motivation for including this component is a possible increase at ~ 0.9 keV in the pulsed fraction as a function of energy. The luminosity of such a region, $\sim 8 \times 10^{29}$ ergs s^{-1}, would most likely be powered by the impact of high-energy particles accelerated in the magnetosphere and flowing down along the open field lines. Alternatively, a larger region with $T_1 = (4 - 12) \times 10^5$ K

and $A_1 < 200$ km^2, might contribute the majority of the *EUVE* and soft X-ray flux, but only if a smaller, hotter component were present as well. Purely thermal models permit values of N_H as low as 10^{19} cm^{-2}.

We are not confident that the existence of a small, thermally emitting region will stand up to detailed modelling which takes into account the magnetic and viewing geometry inferred from the sweep of radio polarization angle. Whereas the modulation due to the thermal component would have to very large to cause an observable energy dependence, the actual modulation from a polar cap may be small because it remains more than 15° above the limb at all times, according to the results of the rotating vector model. This, plus the additional flux bent around the horizon from the opposite polar cap, may conspire to keep the pulsed fraction small. Of course, this potential difficulty could be sidestepped by abandoning the assumption of a simple centered dipole, and assigning the polar caps to arbitrary locations on the star.

One fact that does seem more understandable now than previously is the absence of high-energy γ-ray emission from PSR J0437–4715. Its kinematically corrected spin-down power is only 4×10^{33} ergs s^{-1}, which is an order of magnitude less than that of the lowest-luminosity γ-ray pulsars Geminga and PSR B1055–52. The absence of high-energy γ-rays from PSR J0437–4715 might signify an inefficient or dead outer gap accelerator. If any of the surface thermal X-ray emission from those efficient γ-ray pulsars is due to heating by particles streaming down from their accelerators, then the lack of a more luminous reheated surface on PSR J0437–4715 is not unexpected.

We thank Roger Romani for pointing out the discontinuity in the *ROSAT* timing of the observation of PSR J0437–4715, and David Helfand for helpful discussions and a critical reading of the manuscript. This work was supported by NASA grants NAG 5–1935 and NAG 5–2569. This paper is contribution No. 572 of the Columbia Astrophysics Laboratory.

REFERENCES

Bailyn, C. D. 1993, ApJ, 411, L83
Barret, D., et al. 1994, A&A, 288, 472
Becker, W., & Trümper, J. 1993, Nature, 365, 528
Bell, J. F. 1995, private communication
Bell, J. F., Bailes, M., & Bessell, M. S. 1993, Nature, 364, 603
Bell, J. F., Bailes, M., Manchester, R. N., Weisberg, J. M., & Lyne, A. G. 1995, ApJ, 440, L81
Bowyer, S., et al. 1995, ApJS, in press
Camillo, F., Thorsett, S. E., & Kulkarni, S. R. 1994, ApJ, 421, L15
Chen, K., & Ruderman, M. 1993, ApJ, 408, 179
Danziger, I. J., Baade, D., & Della Valle, M. 1993, A&A, 276, 382
Edelstein, J., Foster, R., & Bowyer, S. 1995, ApJ, in press
Elvis, M., Plummer, D., Schachter, J., & Fabbiano, G. 1992, ApJS, 80, 258
Fierro, J. M., et al. 1995, ApJ, 447, 807
Finley, J. P. 1994, in The Soft X-ray Cosmos, ed. E. M. Schlegel, & R. Petre (New York: AIP), 41
Fruchter, A. S., Bookbinder, J., Garcia, M. R., & Bailyn, C. D. 1992, Nature, 359, 303
Halpern, J. P. & Ruderman, M. 1993, ApJ, 415, 286
Johnston, S., et al. 1993, Nature, 361, 613
Kulkarni, S. R., Phinney, E. S., Evans, C. R., & Hasinger, G. 1992, Nature, 359, 300
Manchester, R. N., & Johnston, S. 1995, ApJ, 441, L65
Manning, R. A., & Willmore, A. P. 1994, MNRAS, 266, 635
Miller, M. C. 1992, MNRAS, 255, 129
Ögelman, H. 1994, in Lives of Neutron Stars, ed. M. A. Alpar et al. (Dordrecht: Kluwer), 101
Predehl, P. 1994, in The *ROSAT* Users' Handbook, ed. U. G. Briel et al. (Garching: Max-Planck-Institut), 59
Romani, R. W. 1987, ApJ, 313, 178
Ruderman, M., Chen, K., Cheng, K. S., & Halpern, J. P. 1993, in Proc. Compton Symposium, ed. M. Friedlander, N. Gehrels, & D. J. Macomb (New York: AIP), 259
Thompson, D. J., et al. 1995, ApJS, in press
Yancopoulos, S., Hamilton, T. T., & Helfand, D. J. 1994, ApJ, 429, 832

FIGURE CAPTIONS

FIG. 1.– Soft X-ray pulse profile of PSR J0437–4715 from the *EUVE* Deep Survey instrument. Background has been subtracted. The phase is arbitrary. Note that the time resolution is at best 0.5 ms, or 2 bins in the light curve. The data are repeated for two cycles to guide the eye. The pulsed fraction is 0.27 ± 0.05.

FIG. 2.– X-ray pulse profile of PSR J0437–4715 in the *ROSAT* PSPC. Background has been subtracted. The phase is arbitrary. The top panel shows all the data in the 0.08–2.0 keV range, and the lower three panels show the same data separated into three energy bands. Pulsed fractions are indicated at the lower left of each panel. The data are repeated for two cycles to guide the eye.

FIG. 3.– Fit of single-component models to the *ROSAT* PSPC spectrum of PSR J0437–4715. The lowest channel displayed was not used in the fit (a) Power-law fit with $\chi^2_\nu = 0.78$, $\alpha = 1.45$, $N_{\rm H} = 9 \times 10^{19}\,{\rm cm}^{-2}$, $L_{\rm X} = 5.0 \times 10^{30}$ ergs s^{-1}. (b) Blackbody fit with $\chi^2_\nu = 3.2$, $T = 1.5 \times 10^6$ K, $N_{\rm H} = 0$.

FIG. 4.– Confidence contours for the power-law fit. The 90% confidence level for the *ROSAT* PSPC spectrum corresponds to the case of two interesting parameters $(\alpha, N_{\rm H})$. The *EUVE* contour corresponds to agreement of the observed count rate in the DS to within ±15% of the value predicted by folding the corresponding *ROSAT* spectrum through the DS effective area curve. The shaded region indicates the spectral range jointly allowed by both instruments.

FIG. 5.– Effective distribution of counts in the *EUVE* DS corresponding to the range of spectral parameters allowed by the joint power-law fit (the shaded region in Figure 4). Integrals under the curves are within ±15% of the observed count rate.

FIG. 6.– Fit of the power law plus blackbody model to the X-ray spectrum of PSR J0437–4715. (a) Raw counts and model spectra folded through the detector response matrix. (b) Unfolded spectral model.

FIG. 7.– Confidence contours for the parameters of the blackbody X-ray component in the power law plus blackbody fit. The 90% confidence level for the *ROSAT* PSPC spectrum corresponds to the case of three interesting parameters $(T, N_{\rm H}, C)$. The contour marked *EUVE* corresponds to agreement of the observed count rate in the DS to within ±15% of the value predicted by folding the corresponding *ROSAT* spectrum through the DS effective area curve. The shaded region indicates the spectral range jointly allowed by both instruments. The dashed lines are the corresponding radii, in meters, of the emitting area at the assumed distance of 140 pc.

FIG. 8.– Fit of the double blackbody model to the X-ray spectrum of PSR J0437–4715. (a) Raw counts and model spectra folded through the detector response matrix. (b) Unfolded spectral model.

FIG. 9.– Confidence contours for the parameters of the softer blackbody X-ray component in the double blackbody fit. The 90% confidence level for the *ROSAT* PSPC spectrum corresponds to the case of three interesting parameters $(T_1, N_{\rm H}, C)$. The contour marked *EUVE* corresponds to agreement of the observed count rate in the DS to within ±15% of the value predicted by folding the corresponding *ROSAT* spectrum through the DS effective area curve. The shaded region indicates the spectral range jointly allowed by both instruments. The dashed lines are the corresponding contours of area A_1, in km^2, of the soft blackbody component at the assumed distance of 140 pc.

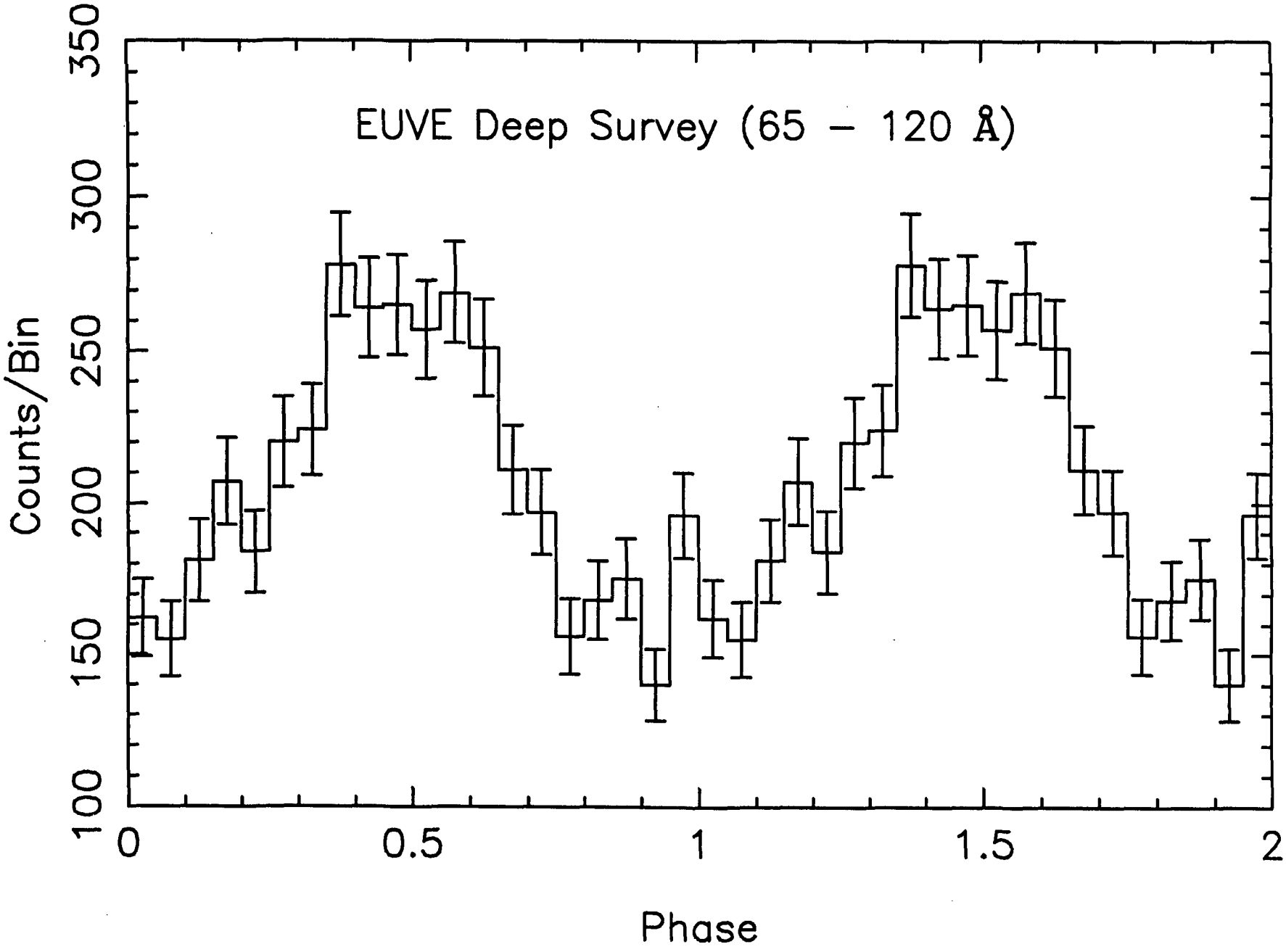
EUVE Deep Survey (65 – 120 Å)
Counts/Bin
100
150
200
250
300
350
0
0.5
1
1.5
2
Phase

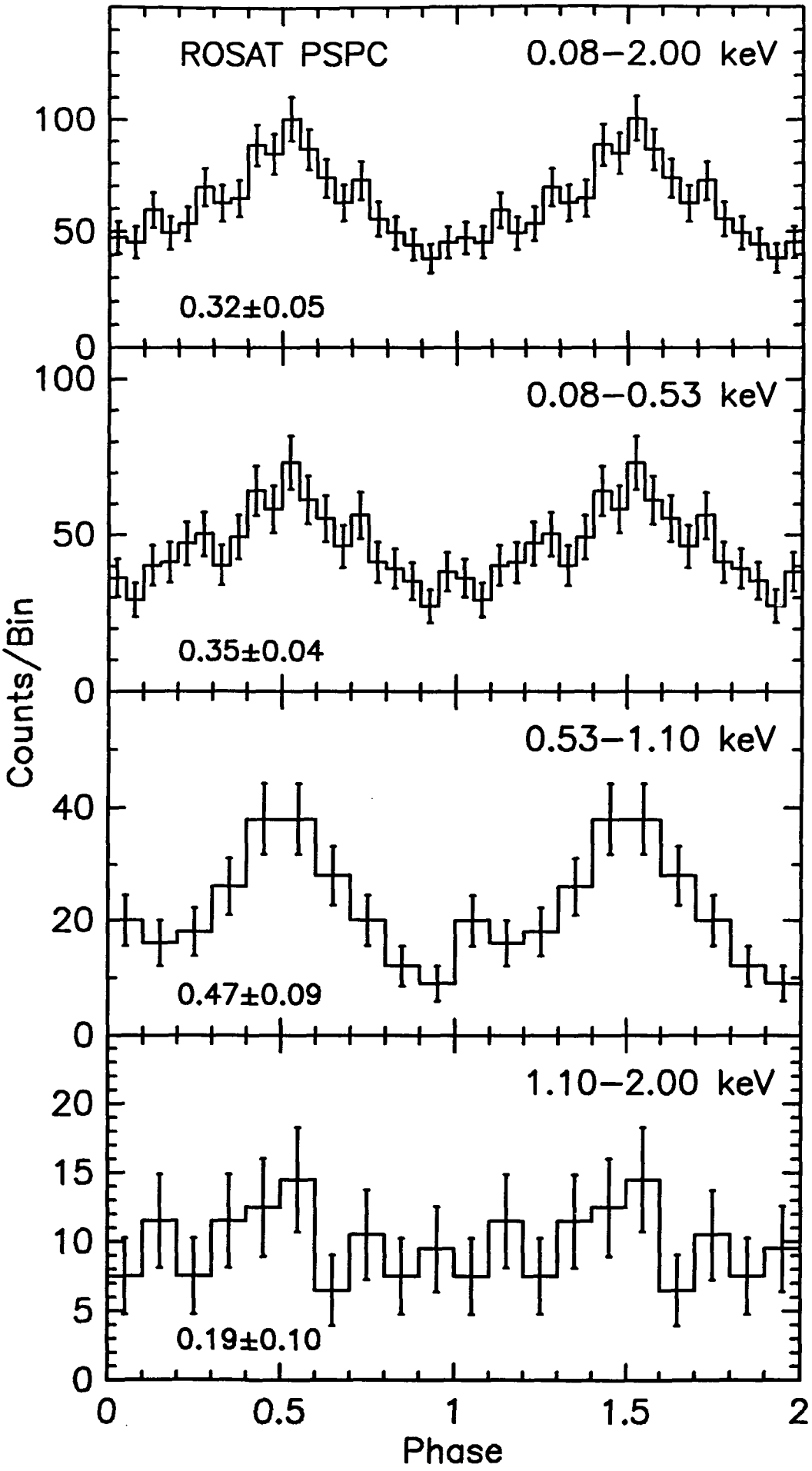
ROSAT PSPC
0.08–2.00 keV
0.32±0.05
0.08–0.53 keV
0.35±0.04
0.53–1.10 keV
0.47±0.09
1.10–2.00 keV
0.19±0.10
Counts/Bin
Phase

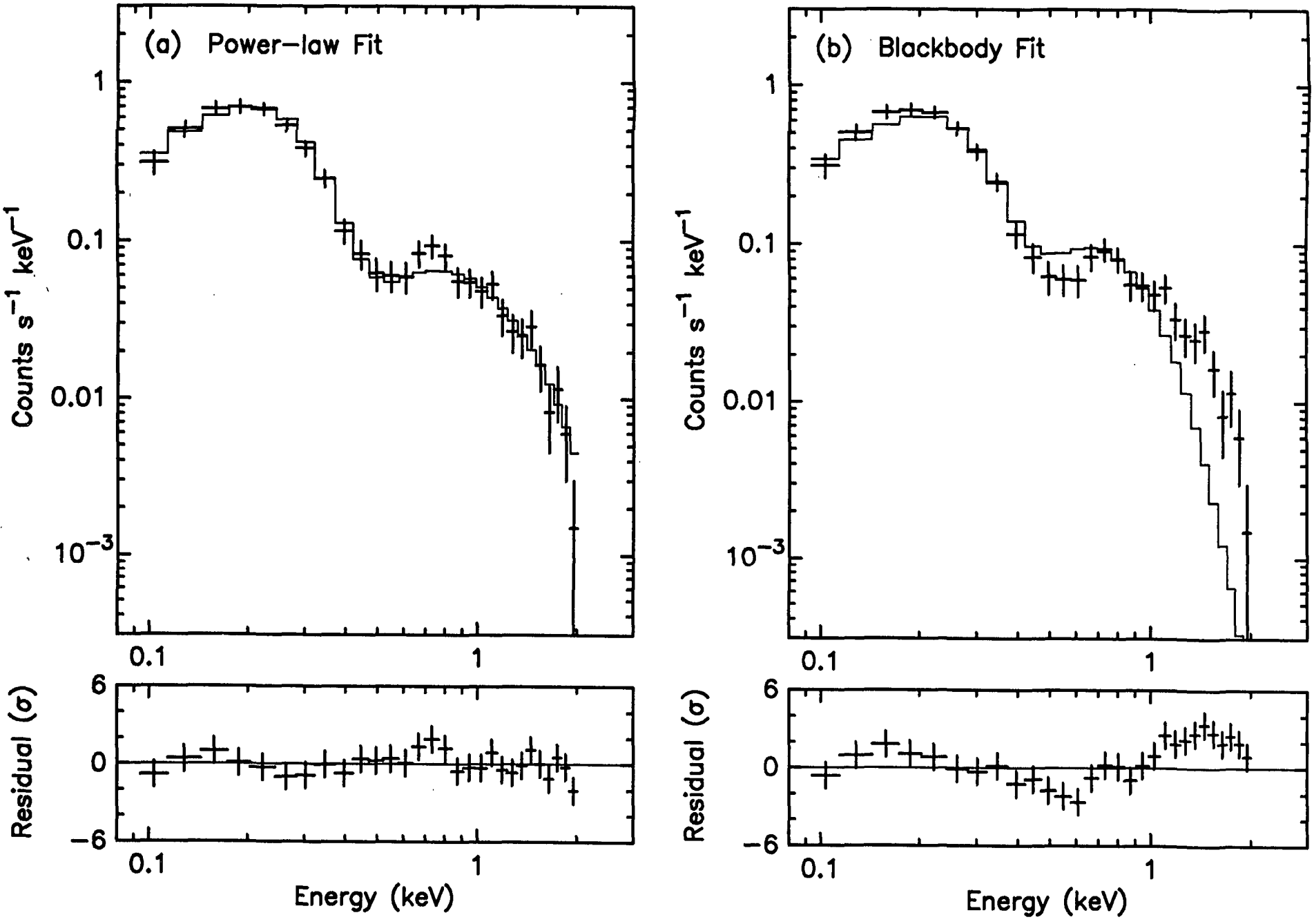
(a) Power-law Fit
(b) Blackbody Fit
Counts s^{-1} keV^{-1}
1
0.1
0.01
10^{-3}
Residual (σ)
6
0
−6
0.1
1
Energy (keV)

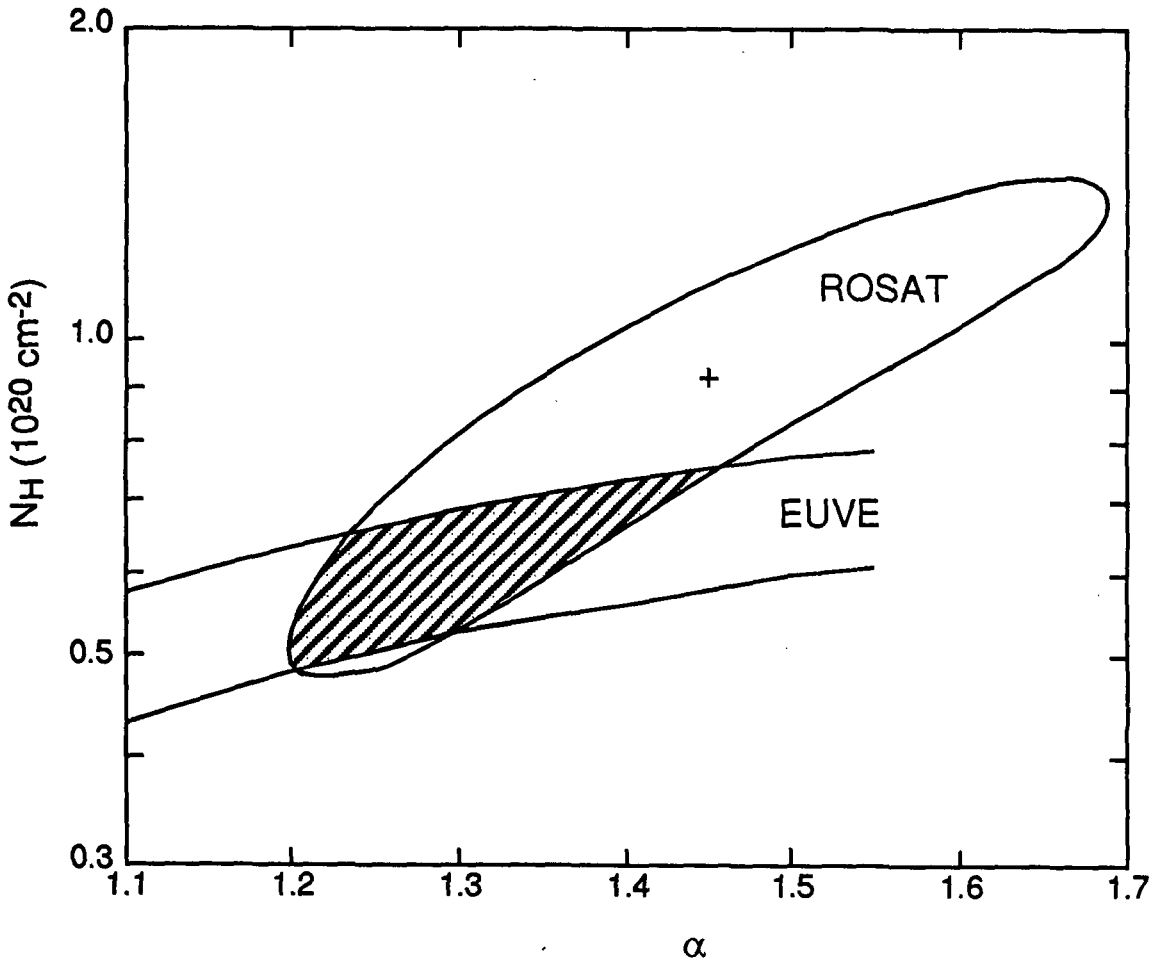
2.0
1.0
0.5
0.3
N_H (10^{20} cm^{-2})
ROSAT
EUVE
1.1
1.2
1.3
1.4
1.5
1.6
1.7
α

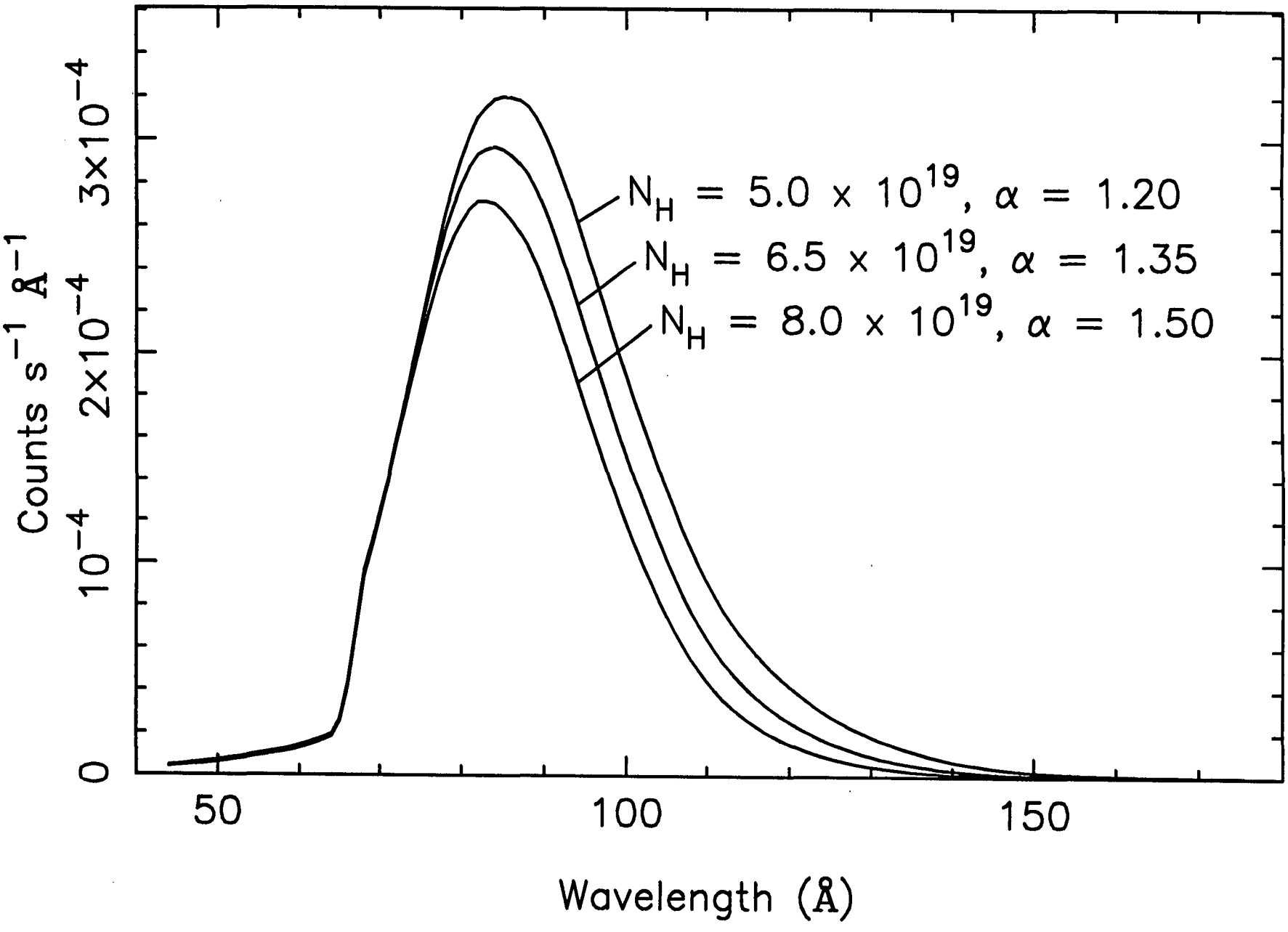
Counts s^{-1} Å^{-1}
0
10^{-4}
2×10^{-4}
3×10^{-4}
50
100
150
Wavelength (Å)
N_H = 5.0 x 10^{19}, α = 1.20
N_H = 6.5 x 10^{19}, α = 1.35
N_H = 8.0 x 10^{19}, α = 1.50

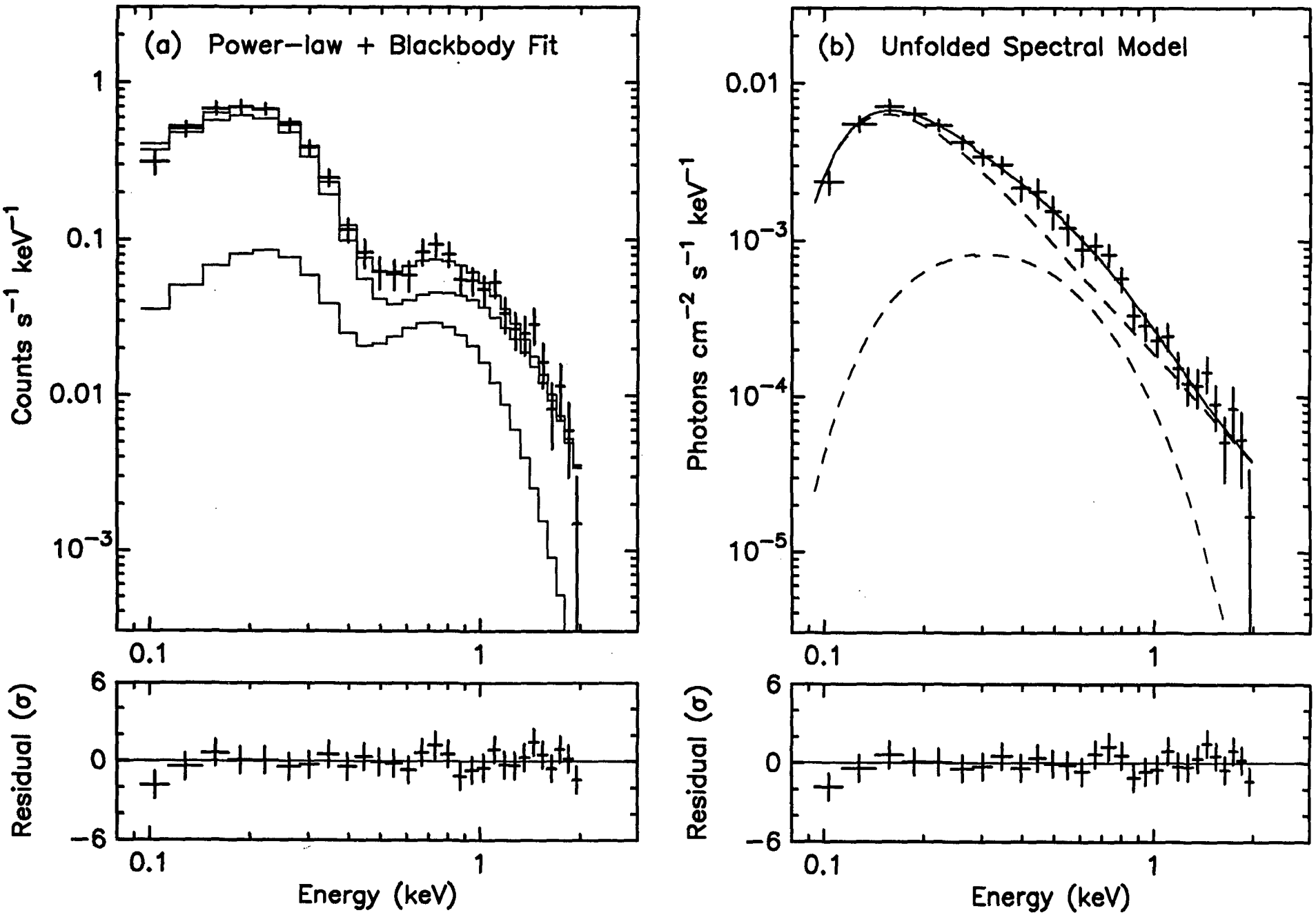
(a) Power–law + Blackbody Fit
Counts s^{-1} keV^{-1}
1
0.1
0.01
10^{-3}
0.1
1
Residual (σ)
6
0
−6
0.1
1
Energy (keV)
(b) Unfolded Spectral Model
Photons cm^{-2} s^{-1} keV^{-1}
0.01
10^{-3}
10^{-4}
10^{-5}
0.1
1
Residual (σ)
6
0
−6
0.1
1
Energy (keV)

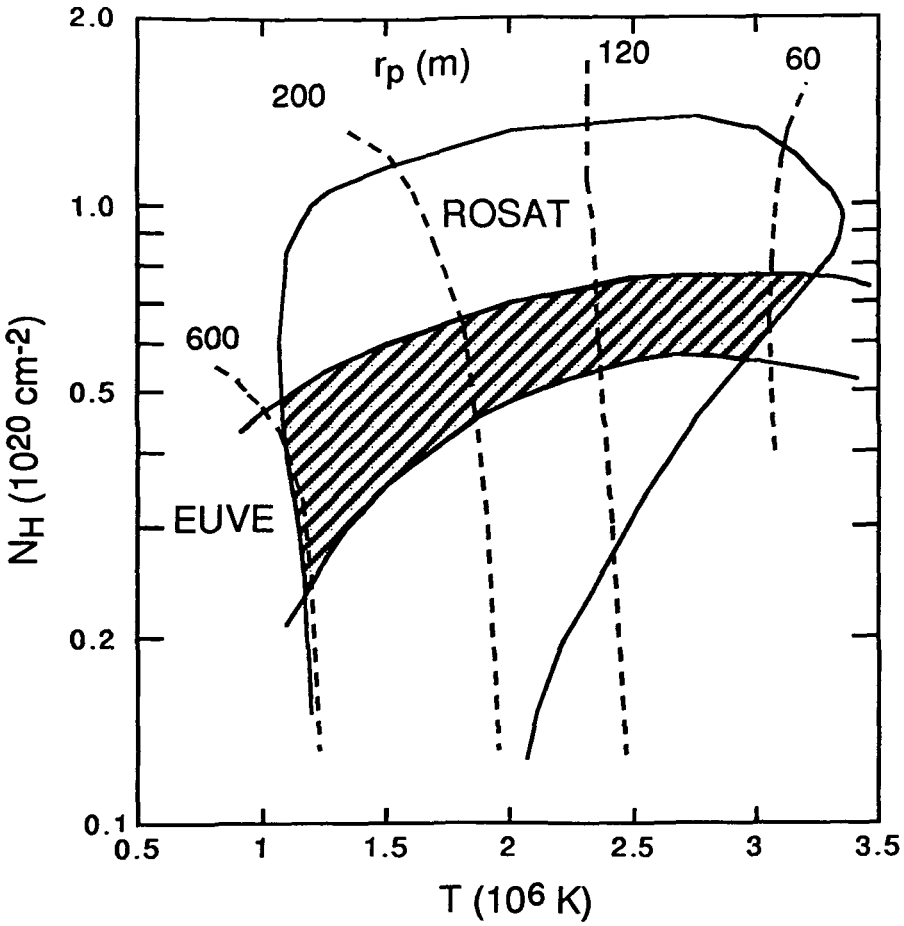
2.0
1.0
0.5
0.2
0.1
N_H (10^{20} cm^{-2})
r_p (m)
200
120
60
600
ROSAT
EUVE
0.5
1
1.5
2
2.5
3
3.5
T (10^6 K)

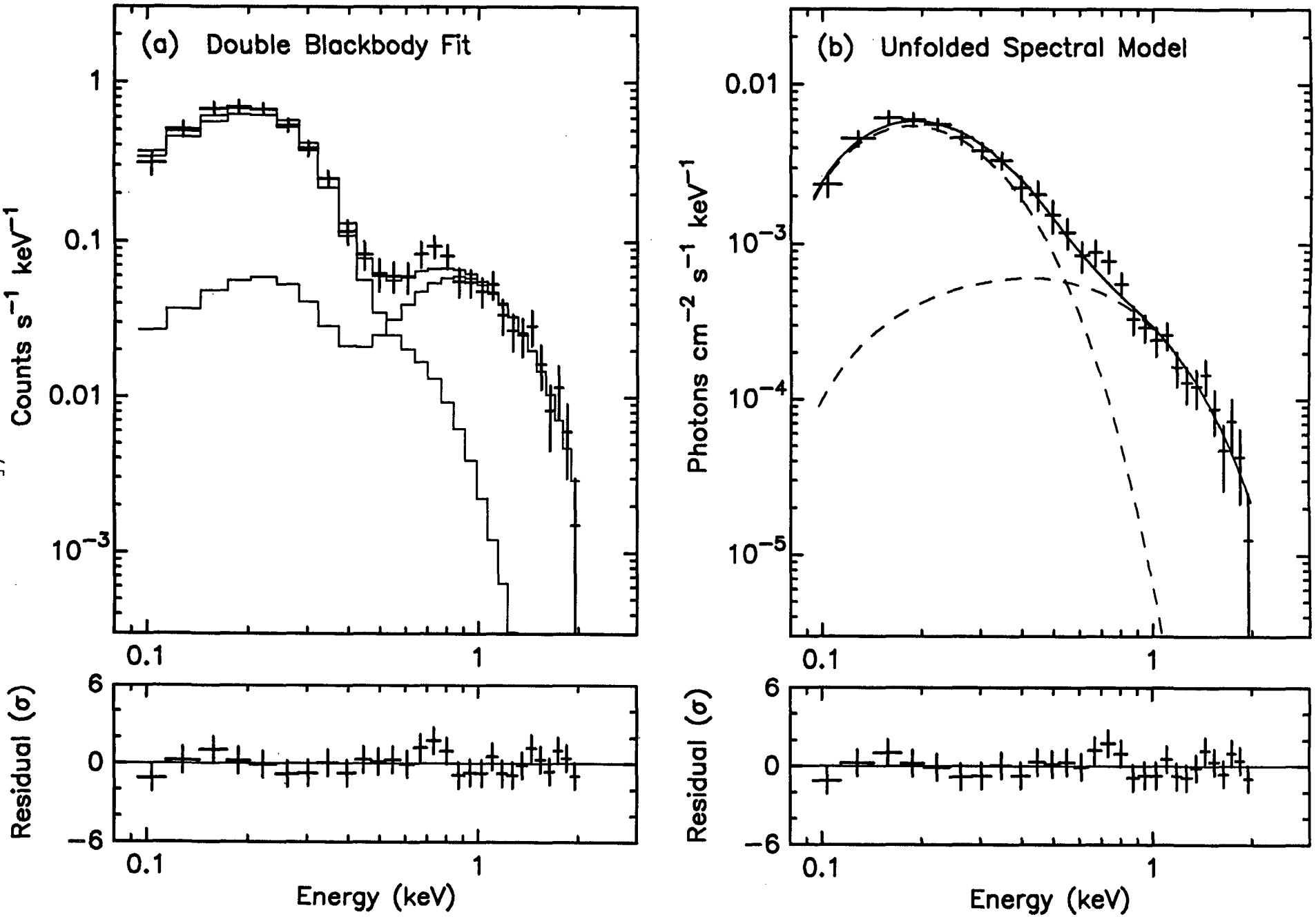
(a) Double Blackbody Fit
Counts s^{-1} keV^{-1}
1
0.1
0.01
10^{-3}
0.1
1
Residual (σ)
6
0
−6
0.1
1
Energy (keV)
(b) Unfolded Spectral Model
Photons cm^{-2} s^{-1} keV^{-1}
0.01
10^{-3}
10^{-4}
10^{-5}
0.1
1
Residual (σ)
6
0
−6
0.1
1
Energy (keV)

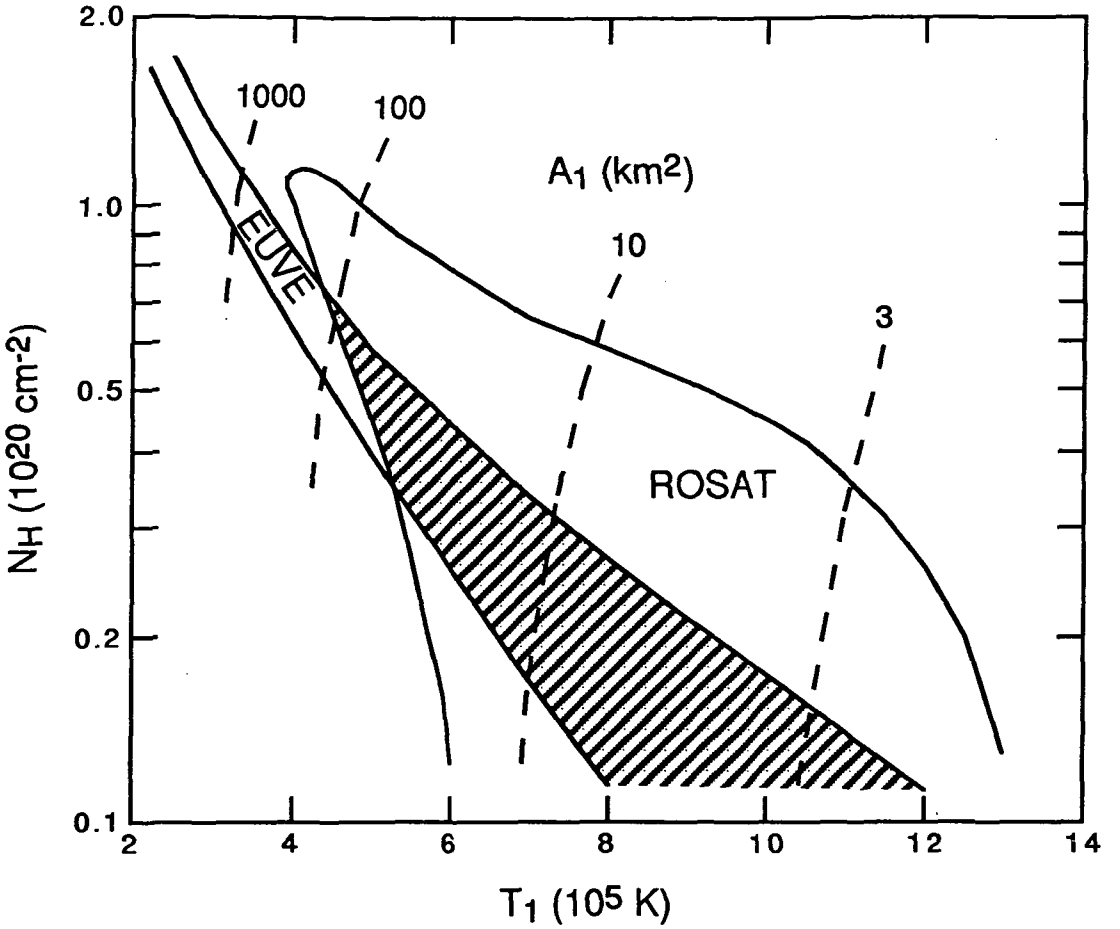
2.0
1.0
0.5
0.2
0.1
2
4
6
8
10
12
14
1000
100
10
3
EUVE
ROSAT
A1 (km2)
NH (1020 cm-2)
T1 (105 K)

OMIT

X-rays from another millisecond pulsar?

SIR — The recent discovery of another nearby millisecond pulsar, PSR J1012+5307[1,2] ($P = 5.26$ ms, $d = 520$ pc), affords a rare opportunity to "see" the surface of an old neutron star via soft X-ray emission from its reheated magnetic polar caps. Only two millisecond pulsars have been detected in X-rays[3–5]. For neither one is it definitely established whether the X-rays are coming from the neutron star's hot surface, or from nonthermal mechanisms in its magnetospheric accelerator. If the former, it would be proof that some mechanism(s) of surface reheating operates in these $\sim 10^9$ yr old pulsars, as all calculations show that neutron stars cool below X-ray emitting temperatures after only 10^6 yr. The location of PSR J1012+5307 in an area of the sky which is particularly deficient in absorbing gas facilitates soft X-ray observations. The column density of neutral hydrogen on the line of sight to PSR J1012+5307 is less than 8×10^{19} cm^{-2}, among the lowest toward any pulsar, and similar to that of the nearest millisecond pulsar PSR J0437–4715[5,6]

In fact, a soft X-ray survey of this favorable area of the sky was already made by the *ROSAT* satellite, in April and May of 1991. In one of those pointed observations, PSR J1012+5307 fell within the field of view of *ROSAT*'s Position Sensitive Proportional Counter, although at a position which is 30′ from the optical axis of the telescope, where the image quality and sensitivity are less than optimal. Within 1′ of the position of the pulsar, we find that there may be a faint source comprising 80 ± 24 photons after background subtraction. If we treat this possible source as either a marginal detection or, more realistically, as an upper limit to the true X-ray flux of the pulsar, it corresponds to a 0.1–2.4 keV luminosity of $\sim 2.5 \times 10^{30}$ erg s^{-1} at the nominal distance of 520 pc[1,2]. A hydrogen column density of 6×10^{19} cm^{-2}, and a spectral index similar to that of PSR J0437–4715[5], were assumed in deriving this upper limit.

Such an X-ray luminosity would be a factor of 2 smaller than that of the nearby PSR J0437–4715[5], and ~ 3 times smaller than that of the "black widow," PSR B1957+20[3,4]. The comparison with the former is particularly significant. Since PSR J0437–4715[7] has

nearly identical spin period and $\dot{P}$ to PSR J1012+5307[2], it can be expected that their X-ray emission mechanisms and luminosities are similar. In both, the X-ray luminosity (or upper limit) is only $\sim 10^{-3}$ times the spin-down power available to the pulsar. The smallness of this number is a basic handicap in testing theories of its origin, as several mechanisms can plausibly account for it. *Pulsed* X-ray emission has only been detected from J0437–4715[5]; even this behaviour has not clearly demonstrated the origin of the X-rays.

The hope for PSRs J1012+5307 and J0437–4715 is that their clear lines of sight will enable future, more sensitive observations to discriminate between thermal and nonthermal origins of their soft X-ray spectra and pulsations. Accurate timing of their soft X-ray pulses may also enable the location of their X-ray emitting regions, e.g., the polar caps of the neutron star, to be determined relative to their radio beams. Furthermore, as all three of these pulsars have binary companions, the role of the companions in their evolutionary history may be prove to be important in understanding their present high-energy emission.

J. P. Halpern

Department of Astronomy,

Columbia University,

538 West 120th Street,

New York, New York 10027, USA

1. Nicastro, L., Lyne, A. G., Lorimer, D. R., Harrison, P. A., Bailes, M. & Skidmore, B. D. *Mon. Not. R. astr. Soc.* **273**, L68–L70 (1995).
2. Lorimer, D. R., Festin, L., Lyne, A. G. & Nicastro, L. *Nature*, in press (1995).
3. Kulkarni, S. R., Phinney, E. S., Evans, C. R. & Hasinger, G. *Nature* **359**, 300–302 (1992).
4. Fruchter, A. S., Bookbinder, J., Garcia, M. R. & Bailyn, C. D. *Nature* **359**, 303–304 (1992).

5. Becker, W. & Trümper, J. *Nature* **365**, 528–530 (1993).

6. Johnston, et al. *Nature* **361**, 613–615 (1993).

7. Bell, J. F., Bailes, M., Manchester, R. N., Weisberg, J. M. & Lyne, A. G. *Astrophys. J. Lett.* **440**, L81–L83 (1995).

APPENDIX

Papers Submitted Under NASA Grant NAG 5-1935

During the Period 1 November 1994 – 31 October 1995

"No X-ray–Luminous Starbursts in the *Einstein* Medium Sensitivity Survey, Either," Halpern, J. P., Helfand, D. J., & Moran, E. C. 1995, *Ap. J.*, in press.

"*ROSAT* PSPC and HRI Observations of the Composite Starburst/Seyefert 2 Galaxy NGC 1672," Brandt, W. N., Halpern, J. P., & Iwasawa, K. 1995, *M.N.R.A.S.*, submitted.

"Soft X-ray Properties of the Binary Millisecond Pulsar J0437-4715," Halpern, J. P., Martin, C., & Marshall, H. L. 1995, *Ap. J.*, submitted.

"X-rays from Another Binary Millisecond Pulsar?," Halpern, J. P. 1995, *Nature*, submitted.

"X-ray Spectra of Cataclysmic Variables from ROSAT," Richman, H. R. 1995, *Ap. J. Suppl.*, in press.